Published in final edited form as:
Semin Nucl Med. 2008 May ; 38(3): 177–198. doi:10.1053/j.semnuclmed.2008.01.001.

Technological Development and Advances in SPECT/CT

Youngho Seo, PhD, **Carina Mari Aparici, MD**, and **Bruce H Hasegawa, PhD**

Abstract

SPECT/CT has emerged over the past decade as a means of correlating anatomical information from CT with functional information from SPECT. The integration of SPECT and CT in a single imaging device facilitates anatomical localization of the radiopharmaceutical to differentiate physiological uptake from that associated with disease and patient-specific attenuation correction to improve the visual quality and quantitative accuracy of the SPECT image. The first clinically available SPECT/CT systems performed emission-transmission imaging using a dual-headed SPECT camera and a low-power x-ray CT sub-system. Newer SPECT/CT systems are available with high-power CT sub-systems suitable for detailed anatomical diagnosis, including CT coronary angiography and coronary calcification that can be correlated with myocardial perfusion measurements. The high-performance CT capabilities also offer the potential to improve compensation of partial volume errors for more accurate quantitation of radionuclide measurement of myocardial blood flow and other physiological processes and for radiation dosimetry for radionuclide therapy. In addition, new SPECT technologies are being developed that significantly improve the detection efficiency and spatial resolution for radionuclide imaging of small organs including the heart, brain, and breast, and therefore may provide new capabilities for SPECT/CT imaging in these important clinical applications.

Introduction

Medical diagnosis is a complex process which relies ultimately on the human perception and intellect to gather information from multiple sources, to sort through many possible actions, and to arrive at the course which best dictates care for an individual patient. Whereas we now rely on a full spectrum of technological innovations that span the discipline of medical imaging, for centuries the only medical image was that gathered by human vision. The most fundamental type of medical imaging was established by Roentgen with the discovery of x-rays one century ago which forever changed the means by which information can be gathered from the human body. Additional advances arose in the 1960s and 1970s when modern medical imaging methods were developed, including Nuclear Medicine (SPECT and PET), computed tomography, digital radiography, and diagnostic ultrasound, and when the fundamentals of nuclear magnetic resonance imaging were established and tested. The development of these technologies has been rapid over the past several decades and has led to use of sophisticated instruments that are both cost-effective and yield diagnostic information that cannot be discerned with unaided human vision. Along with these technological advances, both the quantity and the complexity of information used in the medical diagnostic process have reached levels that were unimaginable even a decade ago. For this reason, it is important to seek and refine technology that not only can increase the information available, but also can assist the diagnostician in synthesizing and relating data that are available from all of these multiple sources.

Diagnosis of disease involves a subtle yet challenging process, one which seeks to identify disorders at the earliest stages of development and biological expression. Imaging methods

such as projection radiography, angiography, computed tomography, magnetic resonance imaging, and ultrasound offer the highest levels of spatial resolution for defining anatomical structures. Furthermore, by administration of contrast media, these methods can visualize blood flow and other functional processes in the cardiovascular, pulmonary, gastrointestinal, urinary, and musculoskeletal systems. However, detection of disease with anatomical imaging methods often requires gross structural changes to be apparent before the diagnosis is definitive. The reliance on anatomical information for diagnosis also makes it difficult to monitor the response of diseased and normal tissues in the critical post-therapy period. In comparison, radiotracer imaging methods such as single photon emission tomography (SPECT) and positron emission tomography (PET) are well-suited to provide critical information about the functional, metabolic, and molecular status of tissues and organs. Radionuclide imaging also can extract measurement data at picomolar and nanomolar concentration levels, rather than the millimolar levels needed for imaging contrast agents with anatomical imaging methods. As a result, subtle and often earlier changes can be detected with targeted radionuclide agents using nuclear imaging than is possible with anatomical imaging methods. While radionuclide imaging has important characteristics for disease detection, it also has well-recognized limitations in spatial resolution and statistical quality [1,2]. Furthermore, while Nuclear Medicine relies on imaging radiopharmaceuticals that are targeted at specific biochemical processes, uptake can occur in both diseased and normal sites and it is important to differentiate these sites to correctly evaluate the patient's status. It therefore has been long recognized and practiced in Nuclear Medicine and Radiology that images acquired using multiple modalities can provide complementary diagnostic information.

A fundamental form of dual-modality imaging occurs when the physician acquires functional (eg SPECT, PET) and anatomic (eg CT, MRI) images of a patient using separate systems. The physician then can view the functional and anatomical images side-by-side on a view box or display monitor to identify complementary features in the images, and thereby extract a decision from that correlated information. However, the practical process of acquiring and spatially (and sometimes temporally) correlating data from two or more imaging systems is complicated by several factors. First, the multiple data sets for an individual generally are acquired on separate days, on different systems, and following unrelated protocols at different locations and by different operators. As a result, operational details of each study may be unknown and such information as well as the images themselves may be difficult to access at a common site. Second, it generally is difficult to maintain the patient in a consistent geometry across separate imaging studies with respect to body position in terms of the curvature of the spine and neck, location of the extremities, the shape of the patient table, the patient respiratory state and cardiac cycle, and shape and status of the patient's gastric, intestinal, and urinary contents. Software techniques have been developed that can register and fuse images from multiple sources [3-7], and are best suited for correlating images from rigid structures such as the brain [8] and skeleton [9,10]. Even when multi-modality image data are available from dual-modality systems, structures within the images can be displaced by respiration, cardiac motion, and other voluntary and involuntary motions. This implies that software-based methods will retain important roles in achieving accurate levels of image registration even when patient studies are performed with PET/CT or SPECT/CT devices [11].

Nevertheless, image registration has proved to be difficult when applied alone in the thorax, abdomen, and pelvis where body structures are elastic and deformable, and can change shape over short periods of time due to internal and external patient motion. The problem of image co-registration is complicated when the images represent fundamentally different information (*eg* PET vs. MRI, SPECT vs. CT) that may offer few commonly-recognizable landmarks and are acquired at different levels of spatial resolution. For these reason, dual-

modality systems [12-19] increasingly are being used to acquire complementary image data with geometrical configurations that are as consistent to one another as possible, and in a way that facilitates the logistics of spatially registering data and then combining or fusing data from multi-modality imaging procedures. These systems have proven beneficial in facilitating attenuation correction of radionuclide data with patient-specific attenuation maps acquired from CT [20-23], and in correlating functional information from the radionuclide image with anatomical studies visualized with CT. Multi-modality image correlation is gaining increased importance in defining treatment planning options for radiation oncology and surgery [7,24-27]. It also promises to have an important role in improving quantitation of radiopharmaceutical uptake [28,29] needed for radiation dosimetry [26,30-32] and to monitor subtle changes such as those needed for assessing therapeutic response and therapeutic monitoring. These recognized capabilities have advanced the use and adoption of dual-modality imaging represented by PET/CT and SPECT/CT.

Dual-Modality Imaging Systems

Direct methods of combining structural and functional information were conceived and implemented in prototype form during the historical beginning of emission and transmission computed tomography, most notably the work by Kuhl, Hale, and Eaton who obtained the first transaxial transmission CT scan of a patient's thorax using their Mark II brain SPECT scanner in the mid-1960s [33]. Despite this pioneering work, the modern use of transmission imaging with external radionuclide transmission sources was not introduced for attenuation correction in SPECT [34,35] and PET [36,37] until the 1980s. The use of external transmission scanning is still used with SPECT to perform both attenuation correction and anatomical localization at sites of radionuclide accumulations. However, this approach has some fundamental limitations, primarily with regard to relatively poor statistical quality which limits the anatomical detail and contrast resolution produced by the transmission scan. As a result, transmission imaging using external radionuclide sources has not achieved routine widespread use with SPECT.

Over the past decade, dual-modality imaging has evolved as a method to facilitate the process of integrating and correlating medical images. For SPECT/CT and PET/CT, such imaging is performed with a system that acquires data from two image modalities supported on a single integrated gantry. The imaging study is performed with the patient remaining on the patient table, which is translated from the CT scanner to the PET or SPECT system to acquire the correlated x-ray and radionuclide image data. The resulting dual-modality image data then can be transferred electronically to a common computer for data correction, reconstruction, display, integration, and analysis. Both SPECT/CT [12,38] and PET/CT systems [16,18,39] are commercially available for clinical as well as pre-clinical imaging. Furthermore, dual-modality PET/MRI systems are under development for small-animal imaging [40,41] and for human brain imaging; SPECT/MRI systems are being developed for pre-clinical imaging of small animal models [42]. (One manufacturer (Gamma Medica) has marketed a tri-modality (PET, SPECT, and CT) device for small-animal imaging.) In comparison to traditional single-modality imaging approaches, the dual-modality systems offer unique capabilities in combining data from two imaging modalities in way that simplifies, yet facilitates, image correlation with the goal of revealing useful diagnostic information that is not easily extracted when the imaging studies are performed independently.

Early Development of SPECT/CT

In the late 1980s, researchers began devising methods to combine radionuclide emission imaging directly with x-ray transmission imaging in a single system. Possibly the earliest

such system was proposed by Mirshanov [43], who received a Soviet patent for a combined transmission-emission tomograph in 1987. This system (Figure 1) was designed so that the patient could undergo simultaneous radionuclide and x-ray imaging with separate scintillation and semiconductor detector viewing the same patient volume, with the resulting emission and transmission data then were recorded with a common image buffer. Although apparently not reduced to practice, this system was perhaps the first that envisioned a combined system with which an x-ray rather than a radionuclide source was integrated directly to produce the transmission data as part of a radionuclide imaging study. Another early design for a dual-modality imaging system was disclosed in an international patent application "Transmission/emission and registered imaging (TERI) computed tomography scanners" by Kaplan [44]. This work proposed acquiring the CT transmission and SPECT emission data simultaneously using imaging detectors (Figure 2) to maintain spatial registration between the two image data sets and to obtain maps of attenuation coefficients to compensate the SPECT data for attenuation. A critical challenge in implementing a simultaneous SPECT/CT system lies in the still-unsolved difficulty of designing a common detector with sufficient temporal and energy resolution to discriminate the primary radionuclide photons from both the x-ray signal and from scatter of the radionuclide photons. Designing a detector capable of simultaneous x-ray and radionuclide imaging remains a fundamental technical barrier in developing a system for truly simultaneous emission and transmission imaging with performance levels matching those achieved with currently available CT and SPECT systems.

The development of experimental SPECT/CT systems was undertaken by Hasegawa et al at the University of California, San Francisco (CSF) in the late 1980s and early 1990s [45,46]. These investigators envisioned a radionuclide imaging system that incorporated a low-power x-ray generator and source for transmission imaging [46]. A prototype system (Figure 3a) included a collimated array of high-purity germanium (HPGe) detectors [47,48] to record photons from both the external x-ray source and the internal radionuclide distribution that then were processed with photon-counting electronics to discriminate the x-ray data (eg produced at 120 kV) and the radionuclide data (eg emitted at 140 keV for ^{99m}Tc). An image (Figure 3b) of a pig administered a myocardial perfusion agent (^{99m}Tc-sestamibi) shows radiopharmaceutical uptake in the myocardium displayed in red superimposed on in the grayscale CT image of the animal [49,50]. The development of the UCSF emission-transmission CT system demonstrated the technical feasibility of acquiring the x-ray and radionuclide image data simultaneously using an HPGe detector array with high-performance photon-counting electronics. However, this system also revealed several important limitations. First, the prototype system had a physically small (ie 24-element) detector that required several hours to acquire both the emission and transmission data. Moreover, the expense of HPGe made it difficult to envision how this detector technology could be implemented practically at a realistic size and cost. Second, the x-ray tube in the prototype system was operated at a very low power level (eg approximately 100-120 kV at 1 mA) but still produced x-ray data with sufficiently high count-rates to cause pulse pile-up that contaminated both the emission and transmission data [51]. The UCSF group designed and tested prototype electronics that allowed the HPGe detector array in the SPECT/CT system to be switched between photon-counting mode for radionuclide imaging and current-mode for x-ray imaging [52-54] for near-simultaneous x-ray and radionuclide imaging using a single detector array. However, it was difficult to envision how such an approach could be cost-effective or practical in a clinical setting. Third, a SPECT/CT system operated with an x-ray tube equivalent to that in a modern CT scanner also would have to account for a roughly 10^7-fold difference in photon fluence encountered in x-ray and radionuclide imaging. For example, a Siemens Somatom x-ray source operated at 125 kV with 2.5-mm aluminum plus 0.4-mm of copper filtration and with a 24° tungsten target produces 3.5×10^6 photons/mAs/mm^2 at a distance of 75 cm [55], or 1.18×10^9 photons/mm^2 at a distance of 1

m when the x-ray tube is operated with a filament current of 600 mA typical of a modern x-ray source. This is equivalent to the photon fluence from a 1.5×10^{16} GBq (4.0×10^{5} Ci) radionuclide source assuming a yield of 1 photon per disintegration (although it is unlikely that a radionuclide source having this strength could be configured physically since self-absorption within the source would limit the photon fluence rate). Similarly, the amount of radioactivity injected in the patient typically is limited by dosimetry concerns to ~20 mCi (740 MBq), or roughly 20-millon-fold lower. Furthermore, the amount of x-ray scatter that occurs within the patient can be estimated roughly as 0.1% of the primary photon fluence, equivalent to a source strength of ~400 Ci (1.5×10^{13} GBq), or a scatter fluence rate 1.2×10^{6} photons/s/mm^2. The photon fluence rates of both the primary and scatter fields are beyond the count-rate capabilities of modern radionuclide imaging system. As a result, it is difficult to envision how a simultaneous SPECT/CT system could be developed with performance matching currently available separate SPECT and CT systems. However, the foregoing analysis helps to emphasize the advantages of transmission imaging with an x-ray versus a radionuclide source in that the former offers faster scans, higher statistics, and better spatial resolution. Furthermore, unlike a radionuclide source, an x-ray source can be turned off and discarded when necessary without any radioactive waste-disposal issues.

The “modern” SPECT/CT system was also originally developed by Hasegawa, et al, at USCF in the mid-1990s [21]. The development of the system grew out of prior experience with the prototype dual-modality system described above which used a single detector to acquire the SPECT/CT data either sequentially or simultaneously. However, as previously discussed, these studies demonstrated the difficulty in acquiring the otherwise incompatible SPECT/CT data simultaneously with a single detector. The modern SPECT/CT system utilizes an alternative approach which has proven to be more robust and incorporates separate state-of-the-art SPECT and CT sub-systems. The SPECT and CT sub-systems can be placed in tandem (ie in-line) for imaging and integrated with a common patient (or animal) table and computer system (Figure 4). This group integrated a GE XR/T SPECT and GE 9800 Quick CT systems with an elongated table that could be positioned for either CT or SPECT imaging [21] without removing the patient from the system. The patient table was mechanically supported with an external brace at the far end of the CT system to minimize downward table deflection when it was extended to the SPECT sub-system. This allowed the CT and SPECT data to be acquired sequentially with the CT data reconstructed in the CT scanner with a conventional filtered backprojection algorithm, then transferred to an external host computer via magnetic tape. The CT data were available for anatomical display, or could be converted (as described below) to obtain a CT-derived map of linear attenuation coefficients to correct the radionuclide data for photon attenuation. The radionuclide projection data acquired with the scintillation camera system were transferred via diskette onto the host computer for iterative reconstruction, allowing the SPECT data to be reconstructed with attenuation correction using the CT-derived attenuation map. These reconstruction and post-processing steps produced three different displays: the x-ray CT data reconstructed from the CT scanner; the radionuclide emission data reconstructed with attenuation correction from the x-ray CT data; and a fused image in which the radionuclide data were displayed in color over a co-registered CT image displayed in grayscale.

Fundamentals of SPECT/CT

Image Registration

Several aspects of the prototype SPECT/CT system remain as important in current SPECT/CT systems, and many of these are important in PET/CT as well. First, the general experience with both SPECT/CT and PET/CT is that dual-modality imaging can simplify the spatial registration of emission and transmission data in comparison to images obtained on separate systems at separate times. This is especially helpful when uptake of a given

radiopharmaceutical is associated with both disease and normal processes. For example, PET accumulation of ^{18}F-FDG occurs in normal heart, brain, kidney, and urinary bladder as well as in regions of inflammation and malignant disease [56,57]. Similarly, SPECT visualized uptake of agents such as ^{111}In-ProstaScint in normal structures such as the prostate, blood pool, and bone marrow, and such uptake can be difficult to differentiate from that associated with prostate carcinoma [58]. By simplifying the process of localizing radiopharmaceutical uptake with CT correlation, dual-modality imaging can help to identify a specific site of radiopharmaceutical accumulation for planning radiation or surgical treatment planning or to differentiate uptake that occurs physiologically from that indicative of disease [14,24,59].

Image registration is improved in dual-modality imaging since the radionuclide and CT data are obtained while the patient maintains the same body position, posture, arm and leg configuration, and table shape during image acquisition. To the extent that the body position remains static throughout image acquisition, this will help to assure accurate image registration even with table translation during the SPECT and CT scanning process. However, the SPECT image acquisition commonly requires 15 to 60 minutes. For myocardial perfusion imaging, the SPECT study requires both rest and stress acquisitions at separate times between which the patient commonly is removed from the table. Similarly, the CT image can be performed within one or a few breath holds with high-performance diagnostic CT, but may require 5 minutes for a low-dose x-ray system. The patient can move, cough, or stretch, or twitch during the scanning process, and internal organs will move due to cardiac or respiratory motion, peristalsis, gas motility, and/or bladder filling [60,61]. Mis-registration errors due to respiratory motion often can be reduced by acquiring the image during quiet tidal respiration which provides fairly consistent acquisitions of the SPECT and CT data. However, the dual-modality acquisitions can exhibit geometrical changes between the SPECT and CT images, making it impossible to simply merge the data without correcting for gross mis-registration errors of several millimeters or more. The primary method of improving image registration relies on image translation following image acquisition and reconstruction, without applying the more subtle transforms of image rotation or regional image warping or shear. Image registration can be applied globally when needed, for example, to compensate for patient table sag, gross patient motion, or mis-calibration between the digital images used to form the CT and SPECT data [62,63]. Current clinical practice continues to rely on the physician's knowledge and experience in interpreting mis-registration errors that remain in the dual-modality image data, generally by comparison of the SPECT data before and following attenuation correction and CT co-registration [64,65]. These studies [64,66] suggest that the combination of SPECT and CT imaging facilitates attenuation correction of myocardial perfusion SPECT with CT co-registration but emphasizes the challenges of translating results from static phantoms to living, breathing patients who move both voluntarily and involuntarily [65,67].

Attenuation Correction

CT can be used to perform attenuation correction of radionuclide emission data since the CT image inherently represents an anatomical map of linear attenuation coefficients (μs) reconstructed at the effective energy of the x-ray beam [20,21,34,35]. This process of generating a map of linear attenuation coefficients in CT is complicated by “beam hardening,” the process in which lower-energy photons are preferentially absorbed as they pass through the patient in a thickness-dependent manner that increases the mean energy in the transmitted x-ray beam emerging from the patient [68,69]. If uncorrected, x-ray beam hardening will, for example, produce images in which the CT values in the center of the body (ie that recorded in the thickest part of the object) are reconstructed with lower attenuation coefficient values than in the periphery, where x-ray absorption is lower and

beam hardening less severe. Modern CT scanners largely account for and correct beam hardening so that a CT scan of uniformly soft tissue regions are reconstructed with uniform image intensity. Beyond normal beam-hardening corrections, when the CT scan is used to derive μ values to correct SPECT (or PET) data for photon attenuation, it must be calibrated so that it represents the linear attenuation coefficients at the photon energy of the radionuclide used to acquire the emission data rather than the mean energy of the x-ray beam used to form the CT image [20-23]. The necessary calibration data can be obtained by acquiring CT scans of a phantom [21] having chambers filled with various concentrations of biologically equivalent materials, for example. air, 60% ethanol (ie a fat simulant), water, normal saline, and various concentrations (ie 50, 100, 200, 300, 400 mg/cm^3) of dipotassium hydrogen phosphate (K_2HPO_4) as a bone-mineral simulant. Alternatively, it is possible to use solid tissue-equivalent materials for the calibration measurement [70]. The CT value of each calibration material then is extracted by defining a region of interest corresponding to each calibration region in the phantom. The linear attenuation coefficient for each such material also can be calculated from the known chemical contents of each region. The calibration data then are represented by relating the extracted image value (in Hounsfield Units, HU) and the calculated linear attenuation coefficient (in units of cm^{-1}) of each calibration material at the photon energy of the γ-rays emitted by the radionuclide source. These data are represented as a piecewise linear calibration curve across the range of image densities seen in clinical CT scans (eg from -1000 to +2000 HU). Typically, the calibration curve is represented as a piecewise bilinear fit in which has different slopes below 0 HU regions of the body which are combinations of air and soft tissue and above 0 HU representing regions which are composed of soft-tissue and bone (Figure 5). The resulting curve is used to convert values in the patient's CT scan from Hounsfield units to those representing the linear attenuation coefficient (ie cm^{-1}) for each CT image pixel. The resulting tomographic image of linear attenuation coefficients (ie commonly known as an “attenuation (or μ) map”) then can be incorporated into an iterative reconstruction algorithm to correct the radionuclide tomogram (ie SPECT or PET image) for errors due to photon attenuation. If only used to correct the radionuclide image for photon attenuation, the CT data can be acquired with a considerably lower statistical quality and coarser spatial resolution than required for diagnostic-quality imaging and therefore can deliver significantly lower dose than that for a diagnostic CT study. However, if improved signal-to-noise performance is needed for direct anatomical diagnosis of the CT scan at higher spatial resolution, including the use of iodine contrast, the anatomical image must be acquired with a diagnostic CT system with a conventional, albeit high, CT radiation dose and spatial resolution.

Patient Table Design

SPECT/CT systems ideally would be designed with all of the radionuclide and x-ray imaging components placed around a common field of view. However, as noted above, the primary x-ray beam used to form the CT image can produce x-ray scatter fluence rate significantly higher than that emitted by the radiopharmaceutical administered to the patient for the emission image. For this reason, modern SPECT/CT (and PET/CT) systems typically separate the imaging planes of the x-ray source and the radionuclide distance by an axial distance of 50 cm or more. This physical separation prevents the primary x-ray beam from striking the radionuclide detectors and minimizes the magnitude of x-ray cross-scatter and related perturbations in the acquisition of radionuclide data of modern SPECT/CT cameras. This requires a patient table that can support the patient while extended between the CT scanner and SPECT sub-system without sagging under the patient's weight and without otherwise vertically displacing the patient between the SPECT and CT imaging positions. As a result, the patient table must be designed with minimal sag while extended for imaging with the SPECT/CT system. Often, table deflection is minimized by supporting the table on

both ends in a way that allows the acquired SPECT and CT data to be spatially correlated and co-registered in a consistent way.

Applications and Capabilities of SPECT/CT

Image Quality in SPECT/CT

Over the past decade, the introduction of SPECT/CT coincided with advances in computing power and iterative reconstruction algorithms and these have led to significant improvements in SPECT image quality obtained. The details of iterative reconstruction in radionuclide imaging have been discussed widely in the scientific literature and will not be repeated here. However, iterative reconstruction methods such as maximum-likelihood expectation-maximization (ML-EM) [71,72] and ordered-subset expectation-maximization (OS-EM) [73-75] offer benefits by allowing incorporation of mathematical models for physical effects [76] that can introduce errors into the SPECT data. These include photon attenuation [50,77], depth-dependent spatial resolution loss (also known as the “geometrical response”) of the radionuclide collimator, and scatter [78-81]. Use of iterative reconstruction for correction of photon attenuation requires an attenuation map derived by transmission imaging with an external radionuclide transmission source or with transmission x-ray imaging with SPECT/CT. X-ray transmission imaging in SPECT/CT also provides a patient-specific map of Compton coefficients that can be used for model-based scatter estimation [78-81] to compensate the radionuclide data for scatter. A final method of improving image quality models the geometrical configuration of the radionuclide collimator (ie including parallel-hole or pinhole collimators) that corrects the SPECT for the geometrical response of the collimator [82-85]. These compensation methods are becoming common for improving the spatial resolution, contrast, and signal-to-noise characteristics of SPECT imaging, including those obtained with SPECT/CT (Figure 6).

Quantitative Accuracy with SPECT/CT

SPECT increasingly is used to quantify the uptake of the radiopharmaceutical in a tumor, the myocardium, or other target region. Typically, this is done by defining volumes-of-interest (Ovis) around the target region to integrate the number of events (ie or counts), assumed to be proportional to the activity in the volume thus defined. The activity (ie in units of MBq or mCi) then is calculated using a calibration factor obtained by imaging a phantom containing a known concentration of the same radionuclide as the radiopharmaceutical used to image the patient. However, as noted, the quantitative accuracy of radionuclide measurements with SPECT can be compromised by several physical factors, attenuation [20,21,35,76,86] and scatter [87-92]. In addition, the quantitative accuracy of SPECT can be compromised by partial-volume errors [93]. That is, the spatial resolution of the radionuclide imaging system causes “spill-out” of radioactivity (ie counts) from the target region into the background and “spill-in” of counts from the background into the target region. These errors are inherent to radionuclide imaging but can be compensated using patient-specific information derived from CT in a SPECT/CT scanner. For example, radionuclide data can be compensated for errors from photon attenuation and scatter radiation [82,94-96] using patient-specific images or “maps” of linear attenuation coefficients derived from CT. When correlated CT data are available, they also can be used to define the size and shape of target regions, and thereby compensate the image of the apparent distribution of activity for partial volume errors caused by the finite spatial resolution of the radionuclide imaging system [32]. Therefore, while it often is noted in the scientific literature that SPECT is not quantitative [97-100] and suffers both accuracy and precision errors, it increasingly is being recognized that SPECT/CT with appropriate reconstruction algorithms can compensate the radionuclide data for photon attenuation, partial volume errors, and scatter radiation [29,76,82,94-96,101] in a

way that significantly improves the accuracy of radionuclide quantitation in comparison to measurements obtained with SPECT alone.

Koral, et al, [31,102] have used correlated SPECT and CT data to quantify the radionuclide content of individual tumor regions. The study acquired SPECT and CT data from separate imaging systems that then were fused in software from patients with non-Hodgkin's lymphoma who were undergoing radioimmunotherapy with ^{131}I-labeled monoclonal antibodies. The quantitation process used CT to derive patient-specific attenuation maps for attenuation correction and CT-defined tumor volumes to correct small (<200 g) tumors for partial-volume correction of the radionuclide data. The shape of the time-activity curve was derived from daily conjugate-view images of a tracer administration of the radiolabeled anti-B_1 antibody. This approach allows estimation of the radionuclide content and therefore the radiation dose delivered to individual tumors that could be resolved with CT but were not necessarily visualized on the conjugate-view scintigraphic images.

Clinical Applications of SPECT/CT

SPECT/CT has been applied and its clinical benefits have been demonstrated across a wide spectrum of applications (Table 1), including both cardiovascular and oncologic imaging. Specifically, correlated CT data facilitate attenuation correction that improves both the contrast [103] and quantitative accuracy of radionuclide imaging performed with SPECT. Furthermore, SPECT/CT provides anatomical data to localize radiotracer uptake and facilitate SPECT diagnoses.

SPECT/CT is important for tumor imaging in terms of improving anatomical localization of disease, helping to define the extent of disease, and improving differentiation of physiological and pathological uptake [14,104-108]. This parallels the clinical experience with ^{18}F-FDG PET and PET/CT imaging.

A role not commonly shared with PET and PET/CT involves of the use of SPECT and SPECT/CT for analyzing radionuclide uptake and radiation dosimetry of tumor-specific SPECT agents in radioimmunotherapy [109-111]. In this setting, SPECT/CT has the potential to improve quantitative accuracy by facilitating the correction for photon attenuation and scatter radiation, as described above. Finally, as also noted above, the size and shape of target regions in the field of view can be quantified and used to correct partial-volume errors in the radionuclide data [30-32]. These methods offer the potential of improving quantitation of radionuclide uptake in and therefore radiation dosimetry of tumor, bone marrow [112], and other normal sites as well as in the targeted tumors in radioimmunotherapy. In addition, the use of the SPECT/CT offers the possibility of calculating patient-specific radiation dose estimates using anatomical information from CT [27,113], rather than relying on generalized anatomic models (such as those used in the Medical Internal Radionuclide Dosimetry (MIRD) formalism).

Myocardial perfusion imaging is a particularly important clinical application of SPECT and therefore is a special focus for SPECT/CT, where a correlated CT-derived map of patient-specific linear attenuation coefficients used to correct the SPECT data for attenuation can potentially introduce false positive defects into the perfusion data. Figure 7 shows an example in which a patient with chest pain was referred for myocardial perfusion SPECT. SPECT data obtained without attenuation correction demonstrated an inferior-wall defect suggestive of right coronary artery disease and the patient was referred to coronary angiography. The SPECT data then were reconstructed with attenuation correction using a CT-derived patient-specific attenuation map obtained from SPECT/CT and were correctly interpreted as normal, as confirmed by the normal coronary angiographic results. A multi-center trial evaluating myocardial perfusion SPECT with ^{99m}Tc-sestamibi or ^{99m}Tc-

tetrofosmin stress imaging in 118 patients found that x-ray-derived attenuation correction obtained with SPECT/CT improved diagnostic interpretation, particularly in normal subjects using coronary angiography as the “gold standard” [114]. Beyond these capabilities for attenuation correction, SPECT/CT with high-performance CT offers the potential for CT coronary angiography that be fused with myocardial imaging performed with SPECT/CT [115-117] or with CT-derived measurements of ventricular function [118,119] as well as the potential to correlate results of radionuclide myocardial perfusion imaging correlated with CT coronary calcium scoring [120]. The latter has been shown to increase the sensitivity of SPECT for detection of coronary artery disease without any significant decrease in specificity. Eventually, it may be possible to use these capabilities to quantify regional myocardial radionuclide uptake and regional myocardial perfusion noninvasively with SPECT/CT [29].

While SPECT with CT-derived attenuation correction can improve the sensitivity, specificity, and diagnostic accuracy of myocardial perfusion imaging [121,122] versus conventional techniques, the accuracy of the results can be affected by registration errors, which are reduced but not eliminated with dual-modality imaging. Specifically, patient motion, including that from respiration and cardiac contraction, during image acquisition can spatially offset the emission and transmission data (Figure 8) and lead to false-positive perfusion defects and other artifacts in the reconstructed SPECT images [67,123]. For example, Tonge et al [63] reconstructed ^{99m}Tc-tetrofosmin SPECT data with x-ray derived attenuation correction. They found that the SPECT data reconstructed from attenuation maps taken directly from the SPECT/CT study contained perfusion defects in the apex and anterior wall, which subsequently were reduced when corrected for registration errors. Furthermore, attenuation corrections reduced the presence of defects in the inferior wall, but were not significantly improved by application of registration correction.

Both phantom and patient studies have shown that spatial displacements between the emission and transmission data of more than 1 pixel (measured in the SPECT image) can compromise the quality of the emission data reconstructed with attenuation correction [60,124]. In one study, Fricke et al [62] found that 27 of 140 patients undergoing ^{99m}Tc-sestamibi SPECT demonstrated pronounced defects in the apical or anterior wall following CT-based attenuation correction. Of the original 27 studies with artifacts, improved co-registration produced normal perfusion patterns in 6 and reduced the presence and severity of defects in 15. No improvement was seen in only 4 of 27 patients; in these studies, the mismatch was less than 1 pixel (7 mm) in the ventro-dorsal direction along which co-registration correction was applied, but had spatial mismatches in the craniocaudal direction which were not corrected [62]. In a separate study with 60 consecutive patients, Goetze et al, found that 42% of the CT attenuation-corrected images had moderate to severe misregistration errors in the SPECT/CT data when evaluated qualitatively [61]. Goetze et al [60] also quantified the spatial mismatch of emission-transmission data from 105 consecutive patients acquired with SPECT/CT and found that 64% of studies exhibited spatial misregistration of 1 pixel or greater. Furthermore, they found significant differences in the segmental distribution of radiotracer distribution between the SPECT images reconstructed prior to and following spatial registration. Software-based methods also have been used to improve anatomical registration of SPECT/CT data and to thereby improve diagnostic evaluation of attenuation-corrected myocardial perfusion SPECT [125] as well as SPECT correlation with CT coronary angiography [116,126]. These techniques have been reported to be feasible and reproducible in demonstrating improved diagnostic evaluation of myocardial perfusion imaging with SPECT/CT and for confirming as well as excluding the functional significance of lesions found with CT coronary angiography [116,126]. While the results to date are preliminary, they point to the need to verify and correct, if possible, the

spatial misregistration of the SPECT image and the CT-based attenuation map and other anatomical information obtained from a SPECT/CT system.

Current SPECT/CT Technologies

The clinical use of dual-modality imaging began with in the commercial introduction of SPECT/CT in 1999 and of PET/CT in 2000, and is continuing to advance rapidly, with approximately 2000 PET/CT systems and almost 1000 SPECT/CT systems currently in use worldwide. An annotated list of clinically approved SPECT/CT systems, as of May 2006, is available on-line[1]. The first commercial SPECT/CT system, the GE Discovery VG Hawkeye, was introduced in 1999 and was based on a GE Discovery VG SPECT system, (designed and introduced originally as the Elscint Varicam), a dual-head variable-geometry SPECT system capable of performing planar scintigraphy, SPECT, and ^{18}F-fluorodeoxyglucose (FDG) coincidence imaging. The x-ray sub-system originally was planned by Elscint but was not released until integrated with the GE Discovery VG with the “Hawkeye option”, an x-ray source operated at 140 kV and 2.5 mA and an x-ray detector operated with a slip ring for continuous-rotation CT acquisition. The Hawkeye sub-system acquires x-ray transmission data with a rotation time of 20 seconds with 2.5 mm in-plane resolution and a slice width of 1-cm or 2.5-mm for one- or four-slice configuration, respectively. The current SPECT/CT system from General Electric Healthcare now has been upgraded as the GE Infinia Hawkeye (Figure 9a). Like the Discovery VG Hawkeye, the Infinia Hawkeye SPECT/CT system incorporates an x-ray source with significantly lower power than a conventional diagnostic CT scanners (which operate at 120-140 kV, 500 mA, and 0.4-s (or faster) rotation speed). Although these first-generation SPECT/CT systems are relatively limited in their spatial resolution, scan speed, and signal-to-noise performance of their CT sub-systems, overall they are well-suited in terms of cost and performance to addressing the needs of attenuation correction and low-resolution anatomical localization and provide useful information that improves diagnostic accuracy compared to SPECT scans alone.

SPECT/CT systems with advanced CT capabilities were introduced in 2004 and now are being adopted in clinical practice. These systems, such as the Siemens Symbia [127] (Figure 9b) and the Philips Precedence (Figure 9c), typically match a dual-head SPECT system with a multi-slice CT scanner having performance similar to that obtained with conventional diagnostic CT (Table 2). The Siemens Symbia is also available with a single-slice low-resolution CT scan for attenuation correction and anatomical mapping or with a diagnostic 2-, 6-, or 16-slice CT. Similarly, the Precedence SPECT/CT system from Philips is available with a 6- or 16 slice CT capability. Both the low- and high-power CT systems available from the commercial vendors can be used to perform attenuation correction and anatomical localization of the radionuclide data suitable for myocardial perfusion measurements, tumor imaging (Figure 10), and other radionuclide studies. However, the improved signal-to-noise characteristics and multi-slice capability of the higher-power CT systems offer detailed anatomical information with improved spatial resolution, excellent soft-tissue contrast resolution, and sufficiently fast scan speed for applications with intravenous iodine contrast enhancement [128]. These characteristics are especially suitable for oncology [14,104-108] where detailed anatomical localization is needed. Other investigators have reported using the higher-performance SPECT/CT systems for applications in orthopedics [129-132], infection and inflammation [133-138], pulmonary function [139,140], and endocrinology[141], where the improved anatomical localization helps identify areas of disease that can be difficult to discriminate with SPECT alone. As previously mentioned, high-resolution CT performance

[1]http://www.advanceforioa.com/sharedresources/advanceforioa/resources/DownloadableResources/AR50106_p58ChartSmart.pdf

also can be used to define target anatomy to improve the quantitation of absolute radionuclide uptake in small lesions such as tumors or in the myocardium.

Finally, a SPECT/CT system with cardiac and coronary CT capability is likely to be well-matched to myocardial perfusion radionuclide measurements, which still account for almost 50% of SPECT imaging. SPECT/CT systems are now available with 64-slice CT subs-systems, capable of ultra-short scan times which “freeze” cardiac motion as required for CT coronary angiography [115,116,126] and calcium scoring [142] (Figure 11). The high-performance SPECT/CT systems also have the potential for absolute quantitation of radionuclide content [29] with corrections for photon attenuation, scatter radiation, and partial-volume errors in a way that could offer accurate non-invasive assessment of regional myocardial blood flow and coronary flow reserve. These capabilities are just beginning to emerge, but are likely to be developed and tested as the capabilities and performance of SPECT/CT mature.

Future Developments in SPECT/CT

The scintillation camera technology currently in use for clinical studies still relies on the technology invented by Hal Anger in 1957 [143]. Nevertheless, SPECT and SPECT/CT is continuing to evolve with the introduction of new technologies that have the potential to improve performance beyond that possible with Anger's pioneering approach. Recent advances in detector technology that incorporate silicon photodiode or solid-state materials offer the potential for improved spatial resolution and energy resolution, with greater stability and more compact size [144-148], compared to conventional camera designs based on photomultiplier tube technology. At this early stage in their development, the use of solid-state and semiconductor detectors has focused on imaging of the heart [145,148], breast [149], and other small organs [150]. Nevertheless, it is likely that as these newer detector technologies will mature, they will become more robust in performance and cost-effectiveness and therefore eventually replace the photomultiplier tube in radionuclide imaging detectors.

Innovative SPECT/CT Designs for Cardiac Imaging

A SPECT protocol for myocardial perfusion imaging can consumes 2.5 hours or more in procedure time, including 40-50 minutes of camera time, (longer if soft-tissue attenuation is suspected and the patient is imaged with prone positioning) [151-153]. Recently, myocardial perfusion cameras have been developed with novel detector and collimator geometries that significantly improve detection efficiency while maintaining or improving spatial resolution for myocardial perfusion imaging in comparison to conventional scintillation camera designs. For example, dedicated nuclear cardiology cameras have been developed by Spectrum Dynamics, Ltd.[2] (Caesarea, Israel) and by Cardiarc, Inc.[3] (Canton, MI) and are designed to acquire myocardial perfusion images in only 2 to 3 minutes (Figure 12) versus the 10 to 15 minutes needed with conventional dual-head SPECT systems. Similar performance now is being reported as a works-in-progress (as of 2007) with a new myocardial SPECT camera developed by GE Healthcare. These new instruments offer significant advantages over conventional SPECT/CT systems in which an-expensive CT scanner remains idle while the slow SPECT scan is completed. The inclusion of a highly efficient SPECT system can decrease the scan time of the SPECT study, and in doing so also increases the utilization of CT and patient throughput compared to conventional SPECT/CT systems. The clinical procedure includes 5-6 minutes needed to acquire the correlated

[2]http://www.spectrum-dynamics.com/
[3]http://www.cardiarc.com/

radionuclide and x-ray data with an efficient SPECT camera plus a modern multi-slice CT system versus the 20-25 minutes required with conventional SPECT technology. The total procedure will be lengthened for acquiring both rest and stress myocardial perfusion data, between which the patient typically leaves the imaging system for administration of the radiopharmaceutical for the second perfusion scan. However, significant reductions in scan time would be obtained if the rest/stress images were obtained with simultaneous dual-isotope imaging in which, for example, the patient first was administered ^{201}Tl at rest followed immediately by exercise or pharmacological stress after which the patient would be injected with the ^{99m}Tc perfusion agent for the stress perfusion study. If the imaging system included a high-performance CT scanner, the radionuclide imaging studies could be followed immediately by CT coronary angiography [115,116,126] and assessment of coronary calcification [142]. It is conceivable that the volumetric CT data also could quantify myocardial thickness to improve the measurement of radionuclide uptake in the myocardium [29]. Both CT coronary angiography and quantitation of myocardial perfusion are illustrative the potential for a high-performance myocardial SPECT/CT with a fast and cost-effective acquisition protocol.

Innovative Breast Imaging with SPECT/CT

Tornai et al [154-157] at Duke University are developing a compact dual-modality SPECT/CT system for dedicated tomographic imaging of the pendant, uncompressed female breast. A prototype system is designed to perform SPECT with a 1.620-cm^2 CZT-based compact gamma camera having 2.5-mm pixels that allow flexible angular positioning with a goniometer. This dual-modality breast imager also includes a flat-panel digital detector coupled to a CsI(Tl) phosphor to perform CT with a quasi-monoenergetic x-ray cone-beam produced with a heavily-filtered tungsten anode. The CT system has a stationary polar orientation and is laterally offset from the center of rotation for imaging pendant, uncompressed breasts that are larger than the detector's field of view. Both the x-ray and radionuclide sub-systems are coupled to a common rotation stage and have a common field of view. As independent systems, both dedicated SPECT and CT have yielded visualization of small lesions in the breast, including those located close to the chest wall [154,158-160]. Results from the combined system show that emission projection images can be contaminated by x-ray scatter photons that artifactually increase the apparent signal in reconstructed emission images. Emission contamination also can increase noise in the transmission image resulting in reduced signal-to-noise ratios in reconstructed CT images. Nevertheless, measurements with the combined system components show that optimal placement of the SPECT and CT sub-systems is limited by physical constraints rather than signal cross-contamination that can occur with a SPECT/CT system that shares a common field of view. Overall, integrating both modalities on a single gantry is designed to simplify data acquisition, SPECT-CT image registration, and necessary image corrections with the goals of correlating radionuclide uptake with anatomical structure, improving detection and staging of cancer, monitoring treatment response, and improving selection of surgical biopsy sites.

Concluding Remarks

As we emerge from the first decade of the clinical use of SPECT/CT, several challenges still remain. First, unlike PET/CT, which has essentially replaced PET-only systems commercially, SPECT/CT has not achieved comparable commercial dominance over conventional SPECT. This likely is due in part to the clinical flexibility of SPECT, which is used for a wide spectrum of clinical applications with different radiopharmaceuticals. This is a decidedly different situation than that with PET and PET/CT, which are used predominantly for tumor imaging with ^{18}F-fluorodeoxyglucose. Secondly, as noted above, SPECT/CT suffers an imbalance in cost-effectiveness due to the differences in acquisition

time between SPECT and modern CT. However, as also noted above, advances in SPECT instrumentation, CT technology, and radiopharmaceutical development have the potential to advance SPECT/CT beyond its current level of performance. Potential clinical applications of SPECT/CT are numerous and include more efficient studies of myocardial perfusion imaging with the potential for correlation with CT coronary angiography. CT also has the potential to provide anatomically guided partial-volume correction for absolute quantitation of tumor uptake and dosimetry of tumor-specific agents with an accuracy not achievable using SPECT alone. SPECT/CT also has the potential to advance imaging application in infectious diseases, orthopedics, neurology, and breast cancer. Finally, on the horizon, is the potential for SPECT imaging with new tumor-specific agents now entering clinical trials. Given these characteristics and potential applications, it is likely that the clinical use of SPECT/CT will expand, becoming an increasingly important tool in diagnostic imaging for a wide spectrum of disease.

Acknowledgments

The authors gratefully acknowledge support from Grants 1 R21 HL083073, 5 R21 EB006373, 5 K25 CA114254, 5 R01 EB000288, 2 R44 CA095936, 4 R44 EB001685, 2 R44 H083494, 2 R44 ES012361, and 1 R41 AG030241 from the National Institutes of Health, Grant FG02-07ER84903 from the Department of Energy, Grants dig04-10174 and dig06-10210 from the UC Discovery Grant Program, Grant A107695 from the University of California, Berkeley, Award number 02821-6 from the Thrasher Research Fund, and from General Electric Healthcare, Inc., Philips Medical Systems, Inc., Siemens Medical Solutions, Inc., and Radiation Monitoring Devices.

References

1. Cherry, SR.; Sorenson, JA.; Phelps, ME. Physics in Nuclear Medicine. Philadelphia: Saunders; 2003.
2. Jaszczak RJ, Coleman RE, Lim CB. SPECT: Single photon emission computed tomography. IEEE Tran Nucl Sci 1980;NS-27:1137–1153.
3. Loats H. CT and SPECT image registration and fusion for spatial localization of metastatic processes using radiolabeled monoclonals. J Nucl Med 1993;34:562–566. [PubMed: 8441058]
4. Maintz JB, Viergever MA. A survey of medical image registration. Med Image Anal 1998;2:1–36. [PubMed: 10638851]
5. Hill DL, Batchelor PG, Holden M, Hawkes DJ. Medical image registration. Phys Med Biol 2001;46:R1–45. [PubMed: 11277237]
6. Hutton BF, Braun M, Thurfjell L, Lau DYH. Image registration: an essential tool for Nuclear Medicine. Eur J Nucl Med Mol Imaging 2002;29:559–577. [PubMed: 11914898]
7. Kessler ML. Image registration and data fusion in radiation therapy. Br J Radiol 2006;79(Spec No 1):S99–108. [PubMed: 16980689]
8. Gholipour A, Kehtarnavaz N, Briggs R, Devous M, Gopinath K. Brain functional localization: A survey of image registration techniques. IEEE Tran Med Imag 2007;26:427–451.
9. Barratt DC, Penney GP, Chan CS, Slomczykowski M, Carter TJ, Edwards PJ, Hawkes DJ. Self-calibrating 3D-ultrasound-based bone registration for minimally invasive orthopedic surgery. IEEE Trans Med Imaging 2006;25:312–23. [PubMed: 16524087]
10. Ma B, Ellis RE. Robust registration for computer-integrated orthopedic surgery: laboratory validation and clinical experience. Med Image Anal 2003;7:237–50. [PubMed: 12946466]
11. Pietrzyk U. Does PET/CT render software registration obsolete? Nuklearmedizin 2005;44 1:S13–7. [PubMed: 16395973]
12. Hasegawa BH, Wong KH, Iwata K, Barber WC, Hwang AB, Sakdinawat AE, Ramaswamy M, Price DC, Hawkins RA. Dual-modality imaging of cancer with SPECT/CT. Technol Cancer Res Treat 2002;1:449–58. [PubMed: 12625772]
13. Townsend DW, Beyer T. A combined PET/CT scanner: the path to true image fusion. Brit J Radiol 2002;75:S24–S30. [PubMed: 12519732]

14. Keidar Z, Israel O, Krausz Y. SPECT/CT in tumor imaging: technical aspects and clinical applications. Semin Nucl Med 2003;33:205–18. [PubMed: 12931322]
15. Schillaci O, Simonetti G. Fusion imaging in Nuclear Medicine--applications of dual-modality systems in oncology. Cancer Biother Radiopharm 2004;19:1–10. [PubMed: 15068606]
16. Townsend DW, Yap JT, Carney JP, Hall NC. Developments in PET/CT: From concept to practice. Med Phys 2004;31(abst):1694.
17. Schillaci O. Hybrid SPECT/CT: a new era for SPECT imaging? Eur J Nucl Med Mol Imaging 2005;32:521–4. [PubMed: 15747153]
18. von Schulthess GK, Steinert HC, Hany TF. Integrated PET/CT: current applications and future directions. Radiology 2006;238:405–22. [PubMed: 16436809]
19. Tagliabue L, Schillaci O. SPECT/CT in oncology: the fusion of two imaging modalities is a new standard of care. Q J Nucl Med Mol Imaging 2007;51:285–9. [PubMed: 17923823]
20. LaCroix KJ, Tsui BMW, Hasegawa BH, Brown JK. Investigation of the use of x-ray CT images for attenuation correction in SPECT. IEEE Trans Nucl Sci 1994;41:2793–2799.
21. Blankespoor SC, Wu X, Kalki K, Brown JK, Tang HR, Cann CE, Hasegawa BH. Attenuation correction of SPECT using x-ray CT on an emission-transmission CT system: Myocardial perfusion assessment. IEEE Trans Nucl Sci 1996;43:2263–2274.
22. Kinahan PE, Townsend DW, Beyer T, Sashin D. Attenuation correction for a combined 3D PET/CT scanner. Med Phys 1998;25:2046–2053. [PubMed: 9800714]
23. Kinahan PE, Hasegawa BH, Beyer T. X-ray-based attenuation correction for position tomography/computed tomography scanners. Semin Nucl Med 2003;33:166–179. [PubMed: 12931319]
24. Munley MT, Marks LB, Scarfone C, Sibley GS, Patz EF Jr, Turkington TG, Jaszczak RJ, Gilland DR, Anscher MS, Coleman RE. Multi-modality Nuclear Medicine imaging in three-dimensional radiation treatment planning for lung cancer: challenges and prospects. Lung Cancer 1999;23:105–14. [PubMed: 10217614]
25. Paulino AC, Thorstad WL, Fox T. Role of fusion in radiotherapy treatment planning. Semin Nucl Med 2003;33:238–243. [PubMed: 12931325]
26. Ellis RJ, Kaminsky DA. Fused radioimmunoscintigraphy for treatment planning. Rev Urol 2006;8 1:S11–9. [PubMed: 17021622]
27. Prideaux AR, Song H, Hobbs RF, He B, Frey EC, Ladenson PW, Wahl RL, Sgouros G. Three-dimensional radiobiologic dosimetry: application of radiobiologic modeling to patient-specific 3-dimensional imaging-based internal dosimetry. J Nucl Med 2007;48:1008–16. [PubMed: 17504874]
28. Liu A, Williams LE, Raubitschek AA. A CT assisted method for absolute quantitation of internal radioactivity. Med Phys 1996;23:1919–1228. [PubMed: 8947907]
29. Da Silva AJ, Tang HR, Wong KH, Wu MC, Dae MW, Hasegawa BH. Absolute quantitation of regional myocardial uptake of ^{99m}Tc-sestamibi with SPECT: experimental validation in a porcine model. J Nucl Med 2001;42:772–779. [PubMed: 11337575]
30. Koral KF, Zasadny KR, Kessler ML, Luo JQ, Buchbinder SF, Kaminski MS, Francis I, Wahl RL. CT-SPECT fusion plus conjugate views for determining dosimetry in iodine-131-monoclonal antibody therapy of lymphoma patients. J Nucl Med 1994;35:1714–1720. [PubMed: 7931676]
31. Koral KF, Dewaraja Y, Li J, Barrett CL, Regan DD, Zasadny KR, Rommelfanger SG, Francis IR, Kaminski MS, Wahl RL. Initial results for Hybrid SPECT--conjugate-view tumor dosimetry in ^{131}I-anti-B1 antibody therapy of previously untreated patients with lymphoma. J Nucl Med 2000;41:1579–86. [PubMed: 10994741]
32. Tang HR, Da Silva AJ, Matthay KK, Price DC, Huberty JP, Hawkins RA, Hasegawa BH. Neuroblastoma imaging using a combined CT scanner-scintillation camera and I-131 MIBG. J Nucl Med 2001;42:237–247. [PubMed: 11216522]
33. Kuhl DE, Hale J, Eaton WL. Transmission scanning: A useful adjunct to conventional emission scanning for accurately keying isotope deposition to radiographic anatomy. Radiology 1966;87:278–284. [PubMed: 5915433]
34. Bailey DL, Hutton BF, Walker PJ. Improved SPECT using simultaneous emission and transmission tomography. J Nucl Med 1987;28:844–851. [PubMed: 3494829]

35. Tsui BMW, Gullberg GT, Edgerton ER, Ballard JG, Perry JR, McCartney WH, Berg J. Correction of nonuniform attenuation in cardiac SPECT imaging. J Nucl Med 1989;30:497–507. [PubMed: 2786944]
36. Huang SC, Hoffman EJ, Phelps ME, Kuhl DE. Quantitation in positron emission computed tomography: 2. Effects of inaccurate attenuation correction. J Comput Assist Tomogr 1979;3:804–14. [PubMed: 315970]
37. Carson RE, Daube-Witherspoon ME, Green MV. A method for postinjection PET transmission measurements with a rotating source. J Nucl Med 1988;29:1558–67. [PubMed: 3261786]
38. Bocher M, Balan A, Krausz Y, Shrem Y, Lonn A, Wilk M, Chisin R. Gamma camera-mounted anatomical x-ray tomography: technology, system characteristics, and first images. Eur J Nucl Med 2000;27:619–627. [PubMed: 10901447]
39. Townsend DW, Carney JP, Yap JT, Hall NC. PET/CT today and tomorrow. J Nucl Med 2004;45 1:4S–14S. [PubMed: 14736831]
40. Shao Y, Cherry SR, Farahani K, Meadors K. Simultaneous PET and MR imaging. Phys Med Biol 1997;42:1965–1970. [PubMed: 9364592]
41. Pichler BJ, Judenhofer MS, Catana C, Walton JH, Kneilling M, Nutt RE, Siegel SB, Claussen CD, Cherry SR. Performance test of an LSO-APD detector in a 7-T MRI scanner for simultaneous PET/MRI. J Nucl Med 2006;47:639–47. [PubMed: 16595498]
42. Wagenaar D, Nalcioglu O, Muftuler L, Meier D, Parnham K, Szawlowski M, Kapusta M, Azman S, Gjaerum J, Maehlum G, Wang Y, Tsui B, Patt BE. A multi-ring small animal CZT system for simultaneous SPECT/MRI imaging. J Nuc Med 2007;48(Suppl 2):89P.
43. Mirshanov, DM. Transmission-Emission Computer Tomograph. Tashkent Branch, All-Union Research Surgery Center, USSR Academy of Medical Science; USSR: 1987.
44. Kaplan, CH. Transmission/emission registered image (TERI) computed tomography scanners. International patent application PCT/US90/03722. 1989.
45. Hasegawa BH, Reilly SM, Gingold EL, Cann CE. Design considerations for a simultaneous emission-transmission CT scanner. Radiology 1989;173(P):414.
46. Hasegawa BH, Gingold EL, Reilly SM, Liew SC, Cann CE. Description of a simultaneous emission-transmission CT system. Proc SPIE 1990;1231:50–60.
47. Gutknecht D. Photomask technique for fabricating high purity germanium detectors. Nucl Instr and Meth 1990;288:13–18.
48. Hasegawa BH, Stebler B, Rutt BK, Martinez A, Gingold EL, Barker CS, Faulkner KG, Cann CE, Boyd DP. A prototype high-purity germanium detector system with fast photon-counting circuitry for medical imaging. Med Phys 1991;18:900–9. [PubMed: 1961152]
49. Kalki K, Heanue JA, Blankespoor SC, Wu X, Brown JK, Cann CE, Hasegawa BH, Carver JA, Dae MW, Chin M, Stillson C. A combined SPECT and CT medical imaging system. Proc SPIE 1995;2432:367–375.
50. Kalki K, Blankespoor SC, Brown JK, Hasegawa BH, Dae MW, Chin M, Stillson C. Myocardial perfusion imaging with a combined x-ray CT and SPECT system. J Nucl Med 1997;38:1535–1540. [PubMed: 9379188]
51. Wu X, Brown JK, Kalki K, Hasegawa BH. Characterization and correction of pulse pile-up in simultaneous emission-transmission computed tomography. Med Phys 1996;23:569–575. [PubMed: 9157271]
52. Boles CD, Boser BE, Hasegawa BH, Heanue JA. A multimode digital detector readout for solid-state medical imaging detectors. IEEE J Solid-State Circuits 1998;33:733–742.
53. Heanue, JA. Department of Electrical Engineering and Computer Science. University of California; Berkeley, CA: 1996. Detector and electronics design considerations for an emission-transmission medical imaging system.
54. Heanue JA, Boser BE, Hasegawa BH. CMOS detector readout electronics for an emission-transmission imaging system. IEEE Trans Nucl Sci 1995;42:1133–1138.
55. Birch, R.; Marshall, M.; Adran, GM. Catalogue of spectral data for diagnostic x-rays. London: Hospital Physicists Association; 1979.
56. Rosenbaum SJ, Lind T, Antoch G, Bockisch A. False-positive FDG PET uptake--the role of PET/CT. Eur Radiol 2006;16:1054–65. [PubMed: 16365730]

57. Strauss LG. Fluorine-18 deoxyglucose and false-positive results: a major problem in the diagnostics of oncological patients. Eur J Nucl Med 1996;23:1409–15. [PubMed: 8781149]
58. Schettino CJ, Kramer EL, Noz ME, Taneja S, Padmanabhan P, Lepor H. Impact of fusion of indium-111 capromab pendetide volume data sets with those from MRI or CT in patients with recurrent prostate cancer. AJR Am J Roentgenol 2004;183:519–24. [PubMed: 15269050]
59. Schillaci O. Functional-anatomical image fusion in neuroendocrine tumors. Cancer Biother Radiopharm 2004;19:129–34. [PubMed: 15068621]
60. Goetze S, Brown TL, Lavely WC, Zhang Z, Bengel FM. Attenuation correction in myocardial perfusion SPECT/CT: effects of misregistration and value of reregistration. J Nucl Med 2007;48:1090–5. [PubMed: 17574985]
61. Goetze S, Wahl RL. Prevalence of misregistration between SPECT and CT for attenuation-corrected myocardial perfusion SPECT. J Nucl Cardiol 2007;14:200–6. [PubMed: 17386382]
62. Fricke H, Fricke E, Weise R, Kammeier A, Lindner O, Burchert W. A method to remove artifacts in attenuation-corrected myocardial perfusion SPECT introduced by misalignment between emission scan and CT-derived attenuation maps. J Nucl Med 2004;45:1619–25. [PubMed: 15471824]
63. Tonge CM, Ellul G, Pandit M, Lawson RS, Shields RA, Arumugam P, Prescott MC. The value of registration correction in the attenuation correction of myocardial SPECT studies using low resolution computed tomography images. Nucl Med Commun 2006;27:843–52. [PubMed: 17021423]
64. O'Connor MK, Kemp B, Anstett F, Christian P, Ficaro EP, Frey E, Jacobs M, Kritzman JN, Pooley RA, Wilk M. A multicenter evaluation of commercial attenuation compensation techniques in cardiac SPECT using phantom models. J Nucl Cardiol 2002;9:361–76. [PubMed: 12161711]
65. Wackers FJT. Attenuation compensation of cardiac SPECT: a critical look at a confusing world. J Nucl Cardiol 2002;9:438–40. [PubMed: 12161721]
66. Romer W, Fiedler E, Pavel M, Pfahlberg A, Hothorn T, Herzog H, Bautz W, Kuwert T. Attenuation correction of SPECT images based on separately performed CT: Effect on the measurement of regional uptake values. Nuklearmedizin 2005;44:20–8. [PubMed: 15711725]
67. Takahashi Y, Murase K, Higashino H, Mochizuki T, Motomura N. Attenuation correction of myocardial SPECT images with X-ray CT: effects of registration errors between X-ray CT and SPECT. Ann Nucl Med 2002;16:431–435. [PubMed: 12416584]
68. Herman GT. Correction for beam hardening in computed tomography. Phys Med Biol 1979;24:81–106. [PubMed: 432276]
69. Kijewski PK, Bjarngard BE. Correction for beam hardening in computed tomography. Med Phys 1978;5:209–14. [PubMed: 672814]
70. Hwang AB, Taylor CC, VanBrocklin HF, Dae MW, Hasegawa BH. Attenuation correction of small animal SPECT images acquired with 125I-iodorotenone. IEEE Tran Nucl Sci 2006;53:1213–1220.
71. Lange K, Carson R. EM reconstruction algorithms for emission and transmission tomography. J Comput Assist Tomogr 1984;8:306–316. [PubMed: 6608535]
72. Shepp LA, Vardi Y. Maximum likelihood reconstruction for emission tomography. IEEE Trans Med Imag 1982;MI-1:113–122.
73. Li J, Jaszczak RJ, Greer KL, Coleman RE. Implementation of an accelerated iterative algorithm for cone-beam SPECT. Phys Med Biol 1994;39:643–53. [PubMed: 15551605]
74. Hudson HM, Larkin RS. Accelerated image reconstruction using ordered subsets of projection data. IEEE Trans Med Imag 1994;13:601–609.
75. Romer W, Reichel N, Vija HA, Nickel I, Hornegger J, Bautz W, Kuwert T. Isotropic reconstruction of SPECT data using OSEM3D: correlation with CT. Acad Radiol 2006;13:496–502. [PubMed: 16554230]
76. Zeng GL, Gullberg GT, Tsui BMW, Terry JA. Three-dimensional iterative reconstruction algorithms with attenuation and geometric point response correction. IEEE Trans Nucl Sci 1991;38:693–701.

77. Gullberg GT, Huesman RH, Malko JA, Pelc NJ, Budinger TF. An attenuated projector-backprojector for iterative SPECT reconstruction. Phys Med Biol 1985;30:799–816. [PubMed: 3840265]

78. Beekman FJ, den Harder JM, Viergever MA, van Rijk PP. SPECT scatter modeling in nonuniform attenuating objects. Phys Med Biol 1997;42:1133–1142. [PubMed: 9194133]

79. Frey EC, Tsui BMW. A new method for modeling the spatially-variant, object-dependent scatter response function in SPECT. IEEE Nucl Sci Symp Med Imag Conf Rec 1996;2:1082–1086.

80. Larsson A, Johansson L, Sundstrom T, Riklund Ahlstrom K. A method for attenuation and scatter correction of brain SPECT based on computed tomography images. Nucl Med Comm 2003;24:411–420.

81. Meikle SR, Hutton BF, Bailey DL. A transmission-dependent method for scatter correction in SPECT. J Nucl Med 1994;35:360–7. [PubMed: 8295011]

82. Laurette I, Zeng GL, Welch A, Christian PE, Gullberg GT. A three-dimensional ray-driven attenuation, scatter and geometric response correction technique for SPECT in inhomogeneous media. Phys Med Biol 2000;45:3459–80. [PubMed: 11098917]

83. Beekman FJ, Slijpen ET, de Jong HW, Viergever MA. Estimation of the depth-dependent component of the point spread function of SPECT. Med Phys 1999;26:2311–22. [PubMed: 10587212]

84. Frey EC, Tsui BM, Gullberg GT. Improved estimation of the detector response function for converging beam collimators. Phys Med Biol 1998;43:941–50. [PubMed: 9572517]

85. Formiconi AR, Pupi A, Passeri A. Compensation of spatial system response in SPECT with conjugate gradient reconstruction technique. Phys Med Biol 1989;34:69–84. [PubMed: 2784572]

86. Ficaro EP, Fessler JA, Shreve PD, Kritzman JN, Rose PA, Corbett JR. Simultaneous transmission/emission myocardial perfusion tomography: Diagnostic accuracy of attenuation-corrected Tc-99m-sestamibi single-photon emission computed tomography. Circulation 1996;93:463–473. [PubMed: 8565163]

87. Jaszczak RJ, Greer KL, Floyd CE. Improved SPECT quantitation using compensation for scattered photons. J Nucl Med 1984;25:893–900. [PubMed: 6611390]

88. Koral KF, Wang X, Rogers WL, Clinthorne NH, Wang X. SPECT Compton-scattering correction by analysis of energy spectra. J Nucl Med 1988;29:195–202. [PubMed: 3258023]

89. Mukai T, Links JM, Douglass KH, Wagner HN. Scatter correction in SPECT using non-uniform attenuation data. Phys Med Biol 1988;33:1129–1140. [PubMed: 3264074]

90. Ljungberg M, Strand SE. Attenuation and scatter correction in SPECT for sources in a nonhomogeneous object: a Monte Carlo study. J Nucl Med 1991;32:1278–1284. [PubMed: 2045947]

91. Galt JR, Cullom SJ, Garcia EV. SPECT quantitation: A simplified method of attenuation and scatter correction for cardiac imaging. J Nucl Med 1992;33:2232–2237. [PubMed: 1460522]

92. Frey EC, Tsui BMW. Modeling the scatter response function in inhomogeneous scattering media for SPECT. IEEE Trans Nucl Sci 1994;41:1585–1593.

93. Kessler RM, Ellis JR, Eden M. Analysis of emission tomographic scan data: Limitations imposed by resolution and background. J Comput Assist Tomogr 1984;8:514–522. [PubMed: 6609942]

94. Ljungberg M, Strand S. Scatter and attenuation correction in SPECT using density maps and Monte Carlo simulated scatter functions. J Nucl Med 1990;31:1560–1567. [PubMed: 2395025]

95. Liang Z, Turkington TG, Gilland DR, Jaszczak RJ, Coleman RE. Simultaneous compensation for attenuation, scatter, and detector response for SPECT reconstruction in three dimensions. Phys Med Biol 1992;37:587–603. [PubMed: 1565692]

96. Seo Y, Wong KH, Sun M, Franc BL, Hawkins RA, Hasegawa BH. Correction of Photon Attenuation and Collimator Response for a Body-Contouring SPECT/CT Imaging System. J Nucl Med 2005;46:868–77. [PubMed: 15872362]

97. Germain P, Baruthio J, Roul G, Dumitresco B. First-pass MRI compartmental analysis at the chronic stage of infarction: myocardial flow reserve parametric map. Computers in Cardioloy 2000;27:675–678.

98. Lewis DH, Bluestone JP, Savina M, Zoller WH, Meshberg EB, Minoshima S. Imaging cerebral activity in recovery from chronic traumatic brain injury: a preliminary report. J Neuroimaging 2006;16:272–7. [PubMed: 16808830]

99. Peters AM. Scintigraphic imaging of renal function. Exp Nephrol 1998;6:391–7. [PubMed: 9730654]

100. Sidoti C, Agrillo U. Chronic cortical stimulation for amyotropic lateral sclerosis: a report of four consecutive operated cases after a 2-year follow-up: technical case report. Neurosurgery 2006;58:E384. discussion E384. [PubMed: 16462467]

101. Tsui BMW, Hu HB, Gilland DR, Gullberg GT. Implementation of simultaneous attenuation and detector response correction in SPECT. IEEE Trans Nucl Sci 1988;NS-35:778–783.

102. Koral KF, Dewaraja Y, Li J, Lin Q, Regan DD, Zasadny KR, Rommelfanger SG, Francis IR, Kaminski MS, Wahl RL. Update on hybrid conjugate-view SPECT tumor dosimetry and response in ^{131}I-tositumomab therapy of previously untreated lymphoma patients. J Nucl Med 2003;44:457–464. [PubMed: 12621015]

103. Ruf J, Steffen I, Mehl S, Rosner C, Denecke T, Pape UF, Plotkin M, Amthauer H. Influence of attenuation correction by integrated low-dose CT on somatostatin receptor SPECT. Nucl Med Commun 2007;28:782–8. [PubMed: 17728608]

104. Krausz Y, Keidar Z, Kogan I, Even-Sapir E, Bar-Shalom R, Engel A, Rubinstein R, Sachs J, Bocher M, Agranovicz S, Chisin R, Israel O. SPECT/CT hybrid imaging with ^{111}In-pentetreotide in assessment of neuroendocrine tumours. Clin Endocrinol (Oxf) 2003;59:565–73. [PubMed: 14616879]

105. Hillel PG, van Beek EJ, Taylor C, Lorenz E, Bax ND, Prakash V, Tindale WB. The clinical impact of a combined gamma camera/CT imaging system on somatostatin receptor imaging of neuroendocrine tumours. Clin Radiol 2006;61:579–87. [PubMed: 16784943]

106. Schillaci O, Danieli R, Manni C, Simonetti G. Is SPECT/CT with a hybrid camera useful to improve scintigraphic imaging interpretation? Nucl Med Commun 2004;25:705–10. [PubMed: 15208498]

107. Ingui CJ, Shah NP, Oates ME. Endocrine neoplasm scintigraphy: added value of fusing SPECT/CT images compared with traditional side-by-side analysis. Clin Nucl Med 2006;31:665–72. [PubMed: 17053381]

108. Roach PJ, Schembri GP, Ho Shon IA, Bailey EA, Bailey DL. SPECT/CT imaging using a spiral CT scanner for anatomical localization: Impact on diagnostic accuracy and reporter confidence in clinical practice. Nucl Med Commun 2006;27:977–87. [PubMed: 17088684]

109. Larson SM. Radioimmunology. Imaging and therapy. Cancer 1991;67:1253–1260. [PubMed: 1991286]

110. DeNardo DA, DeNardo GL, Yuan A, Shen S, DeNardo SJ, Macey DJ, Lamborn KR, Mahe M, Groch MW, Erwin WD. Prediction of radiation doses from therapy using tracer studies with iodine-131-labeled antibodies. J Nucl Med 1996;37:1970–1975. [PubMed: 8970516]

111. O'Donoghue JA. Optimal therapeutic strategies for radioimmunotherapy. Recent Results in Cancer Research 1996;141:77–99. [PubMed: 8722421]

112. Boucek JA, Turner JH. Validation of prospective whole-body bone marrow dosimetry by SPECT/CT multi-modality imaging in (^{131})I-anti-CD20 rituximab radioimmunotherapy of non-Hodgkin's lymphoma. Eur J Nucl Med Mol Imaging 2005;32:458–69. [PubMed: 15821965]

113. Song H, Du Y, Sgouros G, Prideaux A, Frey E, Wahl RL. Therapeutic potential of ^{90}Y- and ^{131}I-labeled anti-CD20 monoclonal antibody in treating non-Hodgkin's lymphoma with pulmonary involvement: a Monte Carlo-based dosimetric analysis. J Nucl Med 2007;48:150–7. [PubMed: 17204712]

114. Masood Y, Liu YH, Depuey G, Taillefer R, Araujo LI, Allen S, Delbeke D, Anstett F, Peretz A, Zito MJ, Tsatkin V, Wackers FJ. Clinical validation of SPECT attenuation correction using x-ray computed tomography-derived attenuation maps: multicenter clinical trial with angiographic correlation. J Nucl Cardiol 2005;12:676–86. [PubMed: 16344230]

115. Ghersin E, Keidar Z, Rispler S, Litmanovich D, Bar-Shalom R, Roguin A, Soil A, Israel O, Engel A. Images in cardiovascular medicine. Hybrid cardiac single photon emission computed tomography/computed tomography imaging with myocardial perfusion single photon emission

computed tomography and multidetector computed tomography coronary angiography for the assessment of unstable angina pectoris after coronary artery bypass grafting. Circulation 2006;114:e237–9. [PubMed: 16894043]

116. Gaemperli O, Schepis T, Valenta I, Husmann L, Scheffel H, Duerst V, Eberli FR, Luscher TF, Alkadhi H, Kaufmann PA. Cardiac image fusion from stand-alone SPECT and CT: clinical experience. J Nucl Med 2007;48:696–703. [PubMed: 17475956]
117. Rispler S, Keidar Z, Ghersin E, Roguin A, Soil A, Dragu R, Litmanovich D, Frenkel A, Aronson D, Engel A, Beyar R, Israel O. Integrated single-photon emission computed tomography and computed tomography coronary angiography for the assessment of hemodynamically significant coronary artery lesions. J Am Coll Cardiol 2007;49:1059–67. [PubMed: 17349885]
118. Schepis T, Gaemperli O, Koepfli P, Valenta I, Strobel K, Brunner A, Leschka S, Desbiolles L, Husmann L, Alkadhi H, Kaufmann PA. Comparison of 64-slice CT with gated SPECT for evaluation of left ventricular function. J Nucl Med 2006;47:1288–94. [PubMed: 16883007]
119. Utsunomiya D, Tomiguchi S, Awai K, Shiraishi S, Nakaura T, Yamashita Y. Mutidetector-row CT and quantitative gated SPECT for the assessment of left ventricular function in small hearts: the cardiac physical phantom study using a combined SPECT/CT system. Eur Radiol 2006;16:1818–25. [PubMed: 16456651]
120. Schepis T, Gaemperli O, Koepfli P, Namdar M, Valenta I, Scheffel H, Leschka S, Husmann L, Eberli FR, Luscher TF, Alkadhi H, Kaufmann PA. Added value of coronary artery calcium score as an adjunct to gated SPECT for the evaluation of coronary artery disease in an intermediate-risk population. J Nucl Med 2007;48:1424–30. [PubMed: 17785727]
121. Utsunomiya D, Tomiguchi S, Shiraishi S, Yamada K, Honda T, Kawanaka K, Kojima A, Awai K, Yamashita Y. Initial experience with X-ray CT based attenuation correction in myocardial perfusion SPECT imaging using a combined SPECT/CT system. Ann Nucl Med 2005;19:485–9. [PubMed: 16248385]
122. Fricke E, Fricke H, Weise R, Kammeier A, Hagedorn R, Lotz N, Lindner O, Tschoepe D, Burchert W. Attenuation Correction of Myocardial SPECT Perfusion Images with Low-Dose CT: Evaluation of the Method by Comparison with Perfusion PET. J Nucl Med 2005;46:736–44. [PubMed: 15872344]
123. Tonge CM, Manoharan M, Lawson RS, Shields RA, Prescott MC. Attenuation correction of myocardial SPECT studies using low resolution computed tomography images. Nucl Med Commun 2005;26:231–7. [PubMed: 15722903]
124. Chen J, Caputlu-Wilson SF, Shi H, Galt JR, Faber TL, Garcia EV. Automated quality control of emission-transmission misalignment for attenuation correction in myocardial perfusion imaging with SPECT-CT systems. J Nucl Cardiol 2006;13:43–9. [PubMed: 16464716]
125. Guetter C, Wacker M, Xu C, Hornegger J. Registration of cardiac SPECT/CT data through weighted intensity co-occurrence priors. Med Image Comput Comput Assist Interv Int Conf Med Image Comput Comput Assist Interv 2007;10:725–33.
126. Gaemperli O, Schepis T, Kalff V, Namdar M, Valenta I, Stefani L, Desbiolles L, Leschka S, Husmann L, Alkadhi H, Kaufmann PA. Validation of a new cardiac image fusion software for three-dimensional integration of myocardial perfusion SPECT and stand-alone 64-slice CT angiography. Eur J Nucl Med Mol Imaging 2007;34:1097–106. [PubMed: 17245532]
127. Kappadath SC, Erwin WD, Wendt RE 3rd. Observed inter-camera variability of clinically relevant performance characteristics for Siemens Symbia gamma cameras. J Appl Clin Med Phys 2006;7:74–80. [PubMed: 17533358]
128. Boone JM. Multidetector CT: opportunities, challenges, and concerns associated with scanners with 64 or more detector rows. Radiology 2006;241:334–7. [PubMed: 17057062]
129. Horger M, Eschmann SM, Pfannenberg C, Storek D, Dammann F, Vonthein R, Claussen CD, Bares R. The value of SPET/CT in chronic osteomyelitis. Eur J Nucl Med Mol Imaging 2003;30:1665–73. [PubMed: 14523585]
130. Filippi L, Schillaci O. Usefulness of hybrid SPECT/CT in ^{99m}Tc-HMPAO-labeled leukocyte scintigraphy for bone and joint infections. J Nucl Med 2006;47:1908–13. [PubMed: 17138732]

131. Horger M, Eschmann SM, Pfannenberg C, Storek D, Vonthein R, Claussen CD, Bares R. Added value of SPECT/CT in patients suspected of having bone infection: preliminary results. Arch Orthop Trauma Surg 2007;127:211–21. [PubMed: 17146681]
132. Coutinho A, Fenyo-Pereira M, Dib LL, Lima EN. The role of SPECT/CT with ^{99m}Tc-MDP image fusion to diagnose temporomandibular dysfunction. Oral Surg Oral Med Oral Pathol Oral Radiol Endod 2006;101:224–30. [PubMed: 16448926]
133. Bar-Shalom R, Yefremov N, Guralnik L, Keidar Z, Engel A, Nitecki S, Israel O. SPECT/CT using ^{67}Ga and ^{111}In-labeled leukocyte scintigraphy for diagnosis of infection. J Nucl Med 2006;47:587–94. [PubMed: 16595491]
134. Filippi L, Schillaci O. SPECT/CT with a hybrid camera: a new imaging modality for the functional anatomical mapping of infections. Expert Rev Med Devices 2006;3:699–703. [PubMed: 17280534]
135. Nathan J, Crawford JA, Sodee DB, Bakale G. Fused SPECT/CT imaging of Peri-iliopsoas infection using Indium-111-labeled leukocytes. Clin Nucl Med 2006;31:801–2. [PubMed: 17117077]
136. Ingui CJ, Shah NP, Oates ME. Infection scintigraphy: added value of single-photon emission computed tomography/computed tomography fusion compared with traditional analysis. J Comput Assist Tomogr 2007;31:375–80. [PubMed: 17538282]
137. Filippi L, Biancone L, Petruzziello C, Schillaci O. Tc-99m HMPAO-labeled leukocyte scintigraphy with hybrid SPECT/CT detects perianal fistulas in Crohn disease. Clin Nucl Med 2006;31:541–2. [PubMed: 16921278]
138. Hendrix CW, Fuchs EJ, Macura KJ, Lee LA, Parsons TL, Bakshi RP, Khan WA, Guidos A, Leal JP, Wahl R. Quantitative Imaging and Sigmoidoscopy to Assess Distribution of Rectal Microbicide Surrogates. Clin Pharmacol Ther. 2007
139. Suga K, Kawakami Y, Zaki M, Yamashita T, Shimizu K, Matsunaga N. Clinical utility of co-registered respiratory-gated (^{99m})Tc-Technegas/MAA SPECT-CT images in the assessment of regional lung functional impairment in patients with lung cancer. Eur J Nucl Med Mol Imaging 2004;31:1280–90. [PubMed: 15197501]
140. Suga K, Kawakami Y, Iwanaga H, Tokuda O, Matsunaga N. Automated breath-hold perfusion SPECT/CT fusion images of the lungs. AJR Am J Roentgenol 2007;189:455–63. [PubMed: 17646474]
141. Tan KG, Bartholomeusz FD, Chatterton BE. Detection and follow up of biliary leak on Tc-99m DIDA SPECT-CT scans. Clin Nucl Med 2004;29:642–3. [PubMed: 15365441]
142. Schepis T, Gaemperli O, Koepfli P, Ruegg C, Burger C, Leschka S, Desbiolles L, Husmann L, Alkadhi H, Kaufmann PA. Use of coronary calcium score scans from stand-alone multislice computed tomography for attenuation correction of myocardial perfusion SPECT. Eur J Nucl Med Mol Imaging 2007;34:11–9. [PubMed: 16896667]
143. Anger HO. Scintillation camera. Rev Sci Instru 1957;29:27–33.
144. Despres P, Funk T, Shah KS, Hasegawa BH. Monte Carlo simulations of compact gamma cameras based on avalanche photodiodes. Phys Med Biol 2007;52:3057–74. [PubMed: 17505089]
145. Kubo N, Mabuchi M, Katoh C, Arai H, Morita K, Tsukamoto E, Morita Y, Tamaki N. Validation of left ventricular function from gated single photon computed emission tomography by using a scintillator-photodiode camera: a dynamic myocardial phantom study. Nucl Med Commun 2002;23:639–43. [PubMed: 12089486]
146. Mori I, Takayama T, Motomura N. The CdTe detector module and its imaging performance. Ann Nucl Med 2001;15:487–94. [PubMed: 11831395]
147. Zeng GL, Gagnon D. Image reconstruction algorithm for a spinning strip CZT SPECT camera with a parallel slat collimator and small pixels. Med Phys 2004;31:3461–73. [PubMed: 15651629]
148. Kumita S, Tanaka K, Cho K, Sato N, Nakajo H, Toba M, Fukushima Y, Mizumura S, Takano T, Kumazaki T. Assessment of left ventricular function using solid-state gamma camera equipped with a highly-sensitive collimator. Ann Nucl Med 2003;17:517–20. [PubMed: 14575391]

149. Hruska CB, O'Connor MK, Collins DA. Comparison of small field of view gamma camera systems for scintimammography. Nucl Med Commun 2005;26:441–5. [PubMed: 15838427]

150. Fukumitsu N, Tsuchida D, Ogi S, Uchiyama M, Mori Y, Ooshita T, Narrita H, Yamamoto H, Takeyama H. Use of Digirad 2020tc Imager, a multi-crystal scintillation camera with solid-state detectors in one case for the imaging of autografts of parathyroid glands. Ann Nucl Med 2001;15:533–6. [PubMed: 11831402]

151. Hayes SW, De Lorenzo A, Hachamovitch R, Dhar SC, Hsu P, Cohen I, Friedman JD, Kang X, Berman DS. Prognostic implications of combined prone and supine acquisitions in patients with equivocal or abnormal supine myocardial perfusion SPECT. J Nucl Med 2003;44:1633–40. [PubMed: 14530478]

152. Stowers SA, Umfrid R. Supine-prone SPECT myocardial perfusion imaging: the poor man's attenuation compensation. J Nucl Cardiol 2003;10:338. [PubMed: 12812195]

153. Malkerneker D, Brenner R, Martin WH, Sampson UK, Feurer ID, Kronenberg MW, Delbeke D. CT-based attenuation correction versus prone imaging to decrease equivocal interpretations of rest/stress Tc-99m tetrofosmin SPECT MPI. J Nucl Cardiol 2007;14:314–23. [PubMed: 17556165]

154. Brzymialkiewicz CN, Tornai MP, McKinley RL, Bowsher JE. Evaluation of fully 3-D emission mammotomography with a compact cadmium zinc telluride detector. IEEE Trans Med Imaging 2005;24:868–77. [PubMed: 16011316]

155. Tornai MP, Bowsher JE, Jaszczak RJ, Pieper BC, Greer KL, Hardenbergh PH, Coleman RE. Mammotomography with pinhole incomplete circular orbit SPECT. J Nucl Med 2003;44:583–93. [PubMed: 12679403]

156. Brzymialkiewicz CN, Tornai MP, McKinley RL, Cutler SJ, Bowsher JE. Performance of dedicated emission mammotomography for various breast shapes and sizes. Phys Med Biol 2006;51:5051–64. [PubMed: 16985287]

157. McKinley RL, Tornai MP, Samei E, Bradshaw ML. Simulation study of a quasi-monochromatic beam for x-ray computed mammotomography. Med Phys 2004;31:800–13. [PubMed: 15124997]

158. Tornai MP, McKinley RL, Brzymialkiewicz CN, Madhav P, Cutler SJ, Crotty DJ, Bowsher JE, Samei E, Floyd CE. Design and development of a fully-3D dedicated x-ray computed mammotomography system. Proc SPIE 2005;5745:189–197.

159. McKinley RL, Brzymialkiewicz CN, Madhav P, Tornai MP. Investigation of cone-beam acquisitions implemented using a novel dedicated mammotomography system with unique arbitrary orbit capability. Proc SPIE 2005;5745:609–617.

160. Brzymialkiewicz CN, McKinley RL, Tornai MP. Towards patient imaging with dedicated emission mammotomography. IEEE Nucl Sci Symp Med Imag Conf Rec 2005;3:1519–1523.

161. Even-Sapir E, Keidar Z, Sachs J, Engel A, Bettman L, Gaitini D, Guralnik L, Werbin N, Iosilevsky G, Israel O. The new technology of combined transmission and emission tomography in evaluation of endocrine neoplasms. J Nucl Med 2001;42:998–1004. [PubMed: 11438618]

162. Horger M, Eschmann SM, Pfannenberg C, Vonthein R, Besenfelder H, Claussen CD, Bares R. Evaluation of combined transmission and emission tomography for classification of skeletal lesions. AJR Am J Roentgenol 2004;183:655–61. [PubMed: 15333352]

163. Even-Sapir E. Imaging of malignant bone involvement by morphologic, scintigraphic, and hybrid modalities. J Nucl Med 2005;46:1356–67. [PubMed: 16085595]

164. Goerres GW, Schmid DT, Schuknecht B, Eyrich GK. Bone invasion in patients with oral cavity cancer: comparison of conventional CT with PET/CT and SPECT/CT. Radiology 2005;237:281–7. [PubMed: 16118155]

165. Utsunomiya D, Shiraishi S, Imuta M, Tomiguchi S, Kawanaka K, Morishita S, Awai K, Yamashita Y. Added value of SPECT/CT fusion in assessing suspected bone metastasis: comparison with scintigraphy alone and nonfused scintigraphy and CT. Radiology 2006;238:264–71. [PubMed: 16304081]

166. Even-Sapir E, Metser U, Mishani E, Lievshitz G, Lerman H, Leibovitch I. The detection of bone metastases in patients with high-risk prostate cancer: ^{99m}Tc-MDP Planar bone scintigraphy, single- and multi-field-of-view SPECT, ^{18}F-fluoride PET, and ^{18}F-fluoride PET/CT. J Nucl Med 2006;47:287–97. [PubMed: 16455635]

167. Romer W, Nomayr A, Uder M, Bautz W, Kuwert T. SPECT-guided CT for evaluating foci of increased bone metabolism classified as indeterminate on SPECT in cancer patients. J Nucl Med 2006;47:1102–6. [PubMed: 16818944]

168. Even-Sapir E, Flusser G, Lerman H, Lievshitz G, Metser U. SPECT/multislice low-dose CT: a clinically relevant constituent in the imaging algorithm of nononcologic patients referred for bone scintigraphy. J Nucl Med 2007;48:319–24. [PubMed: 17268031]

169. Schulz V, Nickel I, Nomayr A, Vija AH, Hocke C, Hornegger J, Bautz W, Romer W, Kuwert T. Effect of CT-based attenuation correction on uptake ratios in skeletal SPECT. Nuklearmedizin 2007;46:36–42. [PubMed: 17299653]

170. Filippi L, Schillaci O, Santoni R, Manni C, Danieli R, Simonetti G. Usefulness of SPECT/CT with a hybrid camera for the functional anatomical mapping of primary brain tumors by [Tc^{99m}] tetrofosmin. Cancer Biother Radiopharm 2006;21:41–8. [PubMed: 16480330]

171. Schillaci O, Danieli R, Filippi L, Romano P, Cossu E, Manni C, Simonetti G. Scintimammography with a hybrid SPECT/CT imaging system. Anticancer Res 2007;27:557–62. [PubMed: 17348441]

172. Denecke T, Hildebrandt B, Lehmkuhl L, Peters N, Nicolaou A, Pech M, Riess H, Ricke J, Felix R, Amthauer H. Fusion imaging using a hybrid SPECT-CT camera improves port perfusion scintigraphy for control of hepatic arterial infusion of chemotherapy in colorectal cancer patients. Eur J Nucl Med Mol Imaging. 2005

173. Gruning T, Brogsitter C, Khonsari M, Jones IW, Ormsby PL, Burchert W. X-ray-based attenuation correction of myocardial perfusion scans: practical feasibility and diagnostic impact. Nucl Med Commun 2006;27:853–8. [PubMed: 17021424]

174. Cense HA, Sloof GW, Klaase JM, Bergman JJ, van Hemert FJ, Fockens P, van Lanschot JJ. Lymphatic drainage routes of the gastric cardia visualized by lymphoscintigraphy. J Nucl Med 2004;45:247–52. [PubMed: 14960643]

175. Plotkin M, Wurm R, Eisenacher J, Szerewicz K, Michel R, Schlenger L, Pech M, Denecke T, Kuczer D, Bischoff A, Felix R, Amthauer H. Combined SPECT/CT imaging using ^{123}I-IMT in the detection of recurrent or persistent head and neck cancer. Eur Radiol 2006;16:503–11. [PubMed: 15983775]

176. Plotkin M, Wurm R, Kuczer D, Wust P, Michel R, Denecke T, Ruf J, Schlenger L, Bischoff A, Felix R, Amthauer H. Diagnostic value of ^{123}I-IMT SPECT in the follow-up of head and neck cancer. Onkologie 2006;29:147–52. [PubMed: 16601370]

177. Birchler MT, Thuerl C, Schmid D, Neri D, Waibel R, Schubiger A, Stoeckli SJ, Schmid S, Goerres GW. Immunoscintigraphy of patients with head and neck carcinomas, with an anti-angiogenetic antibody fragment. Otolaryngol Head Neck Surg 2007;136:543–8. [PubMed: 17418248]

178. Schillaci O, Danieli R, Manni C, Capoccetti F, Simonetti G. Technetium-99m-labelled red blood cell imaging in the diagnosis of hepatic haemangiomas: the role of SPECT/CT with a hybrid camera. Eur J Nucl Med Mol Imaging 2004;31:1011–5. [PubMed: 15057491]

179. Zheng JG, Yao ZM, Shu CY, Zhang Y, Zhang X. Role of SPECT/CT in diagnosis of hepatic hemangiomas. World J Gastroenterol 2005;11:5336–41. [PubMed: 16149142]

180. Ikeda O, Kusunoki S, Nakaura T, Shiraishi S, Kawanaka K, Tomiguchi S, Yamashita Y, Takamori H, Chikamoto A, Kanemitsu K. Comparison of fusion imaging using a combined SPECT/CT system and intra-arterial CT: assessment of drug distribution by an implantable port system in patients undergoing hepatic arterial infusion chemotherapy. Cardiovasc Intervent Radiol 2006;29:371–9. [PubMed: 16502168]

181. Sergiacomi G, Schillaci O, Leporace M, Laviani F, Carlani M, Manni C, Danieli R, Simonetti G. Integrated multislice CT and Tc-99m Sestamibi SPECT-CT evaluation of solitary pulmonary nodules. Radiol Med (Torino) 2006;111:213–24. [PubMed: 16671379]

182. Ferran N, Ricart Y, Lopez M, Martinez-Ballarin I, Roca M, Gamez C, Carrerea D, Guirao S, Leon AF, Martin-Comin J. Characterization of radiologically indeterminate lung lesions: ^{99m}Tc-depreotide SPECT versus ^{18}F-FDG PET. Nucl Med Commun 2006;27:507–14. [PubMed: 16710105]

183. Yang A, Xue J, Li X, Yu Y, Deng H, Hu G, Meng X, Li J. Experimental and clinical observations of ^{99m}Tc-MIBI uptake correlate with P-glycoprotein expression in lung cancer. Nucl Med Commun 2007;28:696–703. [PubMed: 17667748]

184. Bar-Shalom R, Yefremov N, Haim N, Dann EJ, Epelbaum R, Keidar Z, Gaitini D, Frenkel A, Israel O. Camera-based FDG PET and ^{67}Ga SPECT in evaluation of lymphoma: comparative study. Radiology 2003;227:353–60. [PubMed: 12637679]

185. Even-Sapir E, Israel O. Gallium-67 scintigraphy: A cornerstone in functional imaging of lymphoma. Eur J Nuc Med Mol Imaging 2003;30:S65–81.

186. Palumbo B, Sivolella S, Palumbo I, Liberati AM, Palumbo R. ^{67}Ga-SPECT/CT with a hybrid system in the clinical management of lymphoma. Eur J Nucl Med Mol Imaging 2005;32:1011–7. [PubMed: 15895228]

187. Kraitchman DL, Tatsumi M, Gilson WD, Ishimori T, Kedziorek D, Walczak P, Segars WP, Chen HH, Fritzges D, Izbudak I, Young RG, Marcelino M, Pittenger MF, Solaiyappan M, Boston RC, Tsui BM, Wahl RL, Bulte JW. Dynamic imaging of allogeneic mesenchymal stem cells trafficking to myocardial infarction. Circulation 2005;112:1451–61. [PubMed: 16129797]

188. Pfannenberg AC, Eschmann SM, Horger M, Lamberts R, Vonthein R, Claussen CD, Bares R. Benefit of anatomical-functional image fusion in the diagnostic work-up of neuroendocrine neoplasms. Eur J Nucl Med Mol Imaging 2003;30:835–43. [PubMed: 12682789]

189. Ozer S, Dobrozemsky G, Kienast O, Beheshti M, Becherer A, Niederle B, Kainberger F, Dudczak R, Kurtaran A. Value of combined XCT/SPECT technology for avoiding false positive planar (^{123})I-MIBG scintigraphy. Nuklearmedizin 2004;43:164–70. [PubMed: 15480505]

190. Amthauer H, Denecke T, Rohlfing T, Ruf J, Bohmig M, Gutberlet M, Plockinger U, Felix R, Lemke AJ. Value of image fusion using single photon emission computed tomography with integrated low dose computed tomography in comparison with a retrospective voxel-based method in neuroendocrine tumours. Eur Radiol 2005;15:1456–62. [PubMed: 15627182]

191. Ikeda O, Tamura Y, Nakasone Y, Shiraishi S, Kawanaka K, Tomiguchi S, Morishita S, Takamori H, Chikamoto A, Kanemitsu K, Yamashita Y. Evaluation of extrahepatic perfusion of anticancer drugs in the right gastric arterial region on fused images using combined CT/SPECT: is extrahepatic perfusion predictive of gastric toxicity? Cardiovasc Intervent Radiol 2007;30:392–7. [PubMed: 17225975]

192. Ikeda O, Tamura Y, Nakasone Y, Shiraishi S, Kawanaka K, Tomiguchi S, Takamori H, Chikamoto A, Kanemitsu K, Yamashita Y. Evaluation of intrahepatic perfusion on fusion imaging using a combined CT/SPECT system: influence of anatomic variations on hemodynamic modification before installation of implantable port systems for hepatic arterial infusion chemotherapy. Cardiovasc Intervent Radiol 2007;30:383–91. [PubMed: 17225972]

193. Ikeda O, Tamura Y, Nakasone Y, Shiraishi S, Kawanaka K, Tomiguchi S, Yamashita Y, Takamori H, Kanemitsu K, Baba H. Comparison of intrahepatic and pancreatic perfusion on fusion images using a combined SPECT/CT system and assessment of efficacy of combined continuous arterial infusion and systemic chemotherapy in advanced pancreatic carcinoma. Cardiovasc Intervent Radiol 2007;30:912–21. [PubMed: 17710478]

194. Kaczirek K, Prager G, Kienast O, Dobrozemsky G, Dudczak R, Niederle B, Kurtaran A. Combined transmission and (^{99m})Tc-sestamibi emission tomography for localization of mediastinal parathyroid glands. Nuklearmedizin 2003;42:220–3. [PubMed: 14571319]

195. Gayed IW, Kim EE, Broussard WF, Evans D, Lee J, Broemeling LD, Ochoa BB, Moxley DM, Erwin WD, Podoloff DA. The value of ^{99m}Tc-sestamibi SPECT/CT over conventional SPECT in the evaluation of parathyroid adenomas or hyperplasia. J Nucl Med 2005;46:248–52. [PubMed: 15695783]

196. Krausz Y, Bettman L, Guralnik L, Yosilevsky G, Keidar Z, Bar-Shalom R, Even-Sapir E, Chisin R, Israel O. Technetium-99m-MIBI SPECT/CT in primary hyperparathyroidism. World J Surg 2006;30:76–83. [PubMed: 16369710]

197. Ruf J, Seehofer D, Denecke T, Stelter L, Rayes N, Felix R, Amthauer H. Impact of image fusion and attenuation correction by SPECT-CT on the scintigraphic detection of parathyroid adenomas. Nuklearmedizin 2007;46:15–21. [PubMed: 17299650]

198. Lavely WC, Goetze S, Friedman KP, Leal JP, Zhang Z, Garret-Mayer E, Dackiw AP, Tufano RP, Zeiger MA, Ziessman HA. Comparison of SPECT/CT, SPECT, and planar imaging with single-

and dual-phase (^{99m})Tc-sestamibi parathyroid scintigraphy. J Nucl Med 2007;48:1084–9. [PubMed: 17574983]

199. Wong TZ, Turkington TG, Polascik TJ, Coleman RE. ProstaScint (capromab pendetide) imaging using hybrid gamma camera-CT technology. AJR Am J Roentgenol 2005;184:676–80. [PubMed: 15671397]
200. Seo Y, Wong KH, Hasegawa BH. Calculation and validation of the use of effective attenuation coefficient for attenuation correction in In-111 SPECT. Med Phys 2005;32:3628–35. [PubMed: 16475761]
201. Seo Y, Franc BL, Hawkins RA, Wong KH, Hasegawa BH. Progress in SPECT/CT imaging of prostate cancer. Technol Cancer Res Treat 2006;5:329–36. [PubMed: 16866563]
202. Ellis RJ, Zhou H, Kim EY, Fu P, Kaminsky DA, Sodee B, Colussi V, Vance WZ, Spirnak JP, Kim C, Resnick MI. Biochemical disease-free survival rates following definitive low-dose-rate prostate brachytherapy with dose escalation to biologic target volumes identified with SPECT/CT capromab pendetide. Brachytherapy 2007;6:16–25. [PubMed: 17284381]
203. Ellis RJ, Zhou H, Kaminsky DA, Fu P, Kim EY, Sodee DB, Colussi V, Spirnak JP, Whalen CC, Resnick MI. Rectal morbidity after permanent prostate brachytherapy with dose escalation to biologic target volumes identified by SPECT/CT fusion. Brachytherapy 2007;6:149–56. [PubMed: 17434109]
204. Sodee DB, Sodee AE, Bakale G. Synergistic value of single-photon emission computed tomography/computed tomography fusion to radioimmunoscintigraphic imaging of prostate cancer. Semin Nucl Med 2007;37:17–28. [PubMed: 17161036]
205. Even-Sapir E, Lerman H, Lievshitz G, Khafif A, Fliss DM, Schwartz A, Gur E, Skornick Y, Schneebaum S. Lymphoscintigraphy for sentinel node mapping using a hybrid SPECT/CT system. J Nucl Med 2003;44:1413–20. [PubMed: 12960185]
206. Belhocine TZ, Scott AM, Even-Sapir E, Urbain JL, Essner R. Role of Nuclear Medicine in the management of cutaneous malignant melanoma. J Nucl Med 2006;47:957–67. [PubMed: 16741305]
207. De Cicco C, Trifiro G, Calabrese L, Bruschini R, Ferrari ME, Travaini LL, Fiorenza M, Viale G, Chiesa F, Paganelli G. Lymphatic mapping to tailor selective lymphadenectomy in cN0 tongue carcinoma: beyond the sentinel node concept. Eur J Nucl Med Mol Imaging 2006;33:900–5. [PubMed: 16604345]
208. Shiraishi S, Tomiguchi S, Utsunomiya D, Kawanaka K, Awai K, Morishita S, Okuda T, Yokotsuka K, Yamashita Y. Quantitative analysis and effect of attenuation correction on lymph node staging of non-small cell lung cancer on SPECT and CT. AJR Am J Roentgenol 2006;186:1450–7. [PubMed: 16632744]
209. Ishihara T, Kaguchi A, Matsushita S, Shiraishi S, Tomiguchi S, Yamashita Y, Kageshita T, Ono T. Management of sentinel lymph nodes in malignant skin tumors using dynamic lymphoscintigraphy and the single-photon-emission computed tomography/computed tomography combined system. Int J Clin Oncol 2006;11:214–20. [PubMed: 16850128]
210. Khafif A, Schneebaum S, Fliss DM, Lerman H, Metser U, Ben-Yosef R, Gil Z, Reider-Trejo L, Genadi L, Even-Sapir E. Lymphoscintigraphy for sentinel node mapping using a hybrid single photon emission CT (SPECT)/CT system in oral cavity squamous cell carcinoma. Head Neck 2006;28:874–9. [PubMed: 16933311]
211. Sherif A, Garske U, de la Torre M, Thorn M. Hybrid SPECT-CT: an additional technique for sentinel node detection of patients with invasive bladder cancer. Eur Urol 2006;50:83–91. [PubMed: 16632191]
212. Keski-Santti H, Matzke S, Kauppinen T, Tornwall J, Atula T. Sentinel lymph node mapping using SPECT-CT fusion imaging in patients with oral cavity squamous cell carcinoma. Eur Arch Otorhinolaryngol 2006;263:1008–12. [PubMed: 16830118]
213. Mar MV, Miller SA, Kim EE, Macapinlac HA. Evaluation and localization of lymphatic drainage and sentinel lymph nodes in patients with head and neck melanomas by hybrid SPECT/CT lymphoscintigraphic imaging. J Nucl Med Technol 2007;35:10–6. quiz 17-20. [PubMed: 17337652]

214. Roarke MC, Ram P, Nguyen BD. Utility of SPECT/CT in preoperative planning for sentinel lymph node biopsy in melanoma and head/neck carcinoma: three illustrative cases. Clin Nucl Med 2007;32:464–5. [PubMed: 17515756]

215. Warncke SH, Mattei A, Fuechsel FG, Z'Brun S, Krause T, Studer UE. Detection rate and operating time required for gamma probe-guided sentinel lymph node resection after injection of technetium-99m nanocolloid into the prostate with and without preoperative imaging. Eur Urol 2007;52:126–32. [PubMed: 17258385]

216. Mattei A, Fuechsel FG, Bhatta Dhar N, Warncke SH, Thalmann GN, Krause T, Studer UE. The template of the primary lymphatic landing sites of the prostate should be revisited: results of a multi-modality mapping study. Eur Urol 2008;53:118–25. [PubMed: 17709171]

217. Nomori H, Ikeda K, Mori T, Shiraishi S, Kobayashi H, Iwatani K, Kawanaka K, Kobayashi T. Sentinel node identification in clinical stage Ia non-small cell lung cancer by a combined single photon emission computed tomography/computed tomography system. J Thorac Cardiovasc Surg 2007;134:182–7. [PubMed: 17599506]

218. Lerman H, Metser U, Lievshitz G, Sperber F, Shneebaum S, Even-Sapir E. Lymphoscintigraphic sentinel node identification in patients with breast cancer: the role of SPECT-CT. Eur J Nucl Med Mol Imaging 2006;33:329–37. [PubMed: 16220303]

219. Lerman H, Lievshitz G, Zak O, Metser U, Schneebaum S, Even-Sapir E. Improved sentinel node identification by SPECT/CT in overweight patients with breast cancer. J Nucl Med 2007;48:201–6. [PubMed: 17268015]

220. Horger M, Eschmann SM, Lengerke C, Claussen CD, Pfannenberg C, Bares R. Improved detection of splenosis in patients with haematological disorders: the role of combined transmission-emission tomography. Eur J Nucl Med Mol Imaging 2003;30:316–9. [PubMed: 12552353]

221. Alvarez R, Diehl KM, Avram A, Brown R, Piert M. Localization of splenosis using ^{99m}Tc-damaged red blood cell SPECT/CT and intraoperative gamma probe measurements. Eur J Nucl Med Mol Imaging 2007;34:969. [PubMed: 17457584]

222. Franzius C, Hermann K, Weckesser M, Kopka K, Juergens KU, Vormoor J, Schober O. Whole-body PET/CT with ^{11}C-meta-hydroxyephedrine in tumors of the sympathetic nervous system: feasibility study and comparison with ^{123}I-MIBG SPECT/CT. J Nucl Med 2006;47:1635–42. [PubMed: 17015899]

223. Yamamoto Y, Nishiyama Y, Monden T, Matsumura Y, Satoh K, Ohkawa M. Clinical usefulness of fusion of ^{131}I SPECT and CT images in patients with differentiated thyroid carcinoma. J Nucl Med 2003;44:1905–10. [PubMed: 14660715]

224. Tharp K, Israel O, Hausmann J, Bettman L, Martin WH, Daitzchman M, Sandler MP, Delbeke D. Impact of ^{131}I-SPECT/CT images obtained with an integrated system in the follow-up of patients with thyroid carcinoma. Eur J Nucl Med Mol Imaging 2004;31:1435–42. [PubMed: 15221294]

225. Ruf J, Lehmkuhl L, Bertram H, Sandrock D, Amthauer H, Humplik B, Ludwig Munz D, Felix R. Impact of SPECT and integrated low-dose CT after radioiodine therapy on the management of patients with thyroid carcinoma. Nucl Med Commun 2004;25:1177–82. [PubMed: 15640775]

226. Minarik D, Sjogreen K, Ljungberg M. A new method to obtain transmission images for planar whole-body activity quantitation. Cancer Biother Radiopharm 2005;20:72–6. [PubMed: 15778584]

227. Mirshanov, DM. USSR Academy of Medical Science. Tashkent Branch, All-Union Research Surgery Center; USSR: 1987. Transmission-emission computer tomograph.

228. Hasegawa BH, Iwata K, Wong KH, Wu MC, Da Silva J, Tang HR, Barber WC, Hwang AH, Sakdinawat AE. Dual-modality imaging of cancer with SPECT/CT. Acad Radiol 2002;9:1305–1321. [PubMed: 12449363]

229. Hasegawa BH, Tang HR, Da Silva AJ, Iwata K, Wu AM, Wong KH. Implementation and applications of a combined CT/SPECT system. IEEE Nucl Sci Symp Med Imag Conf Rec 1999;3:1373–1377.

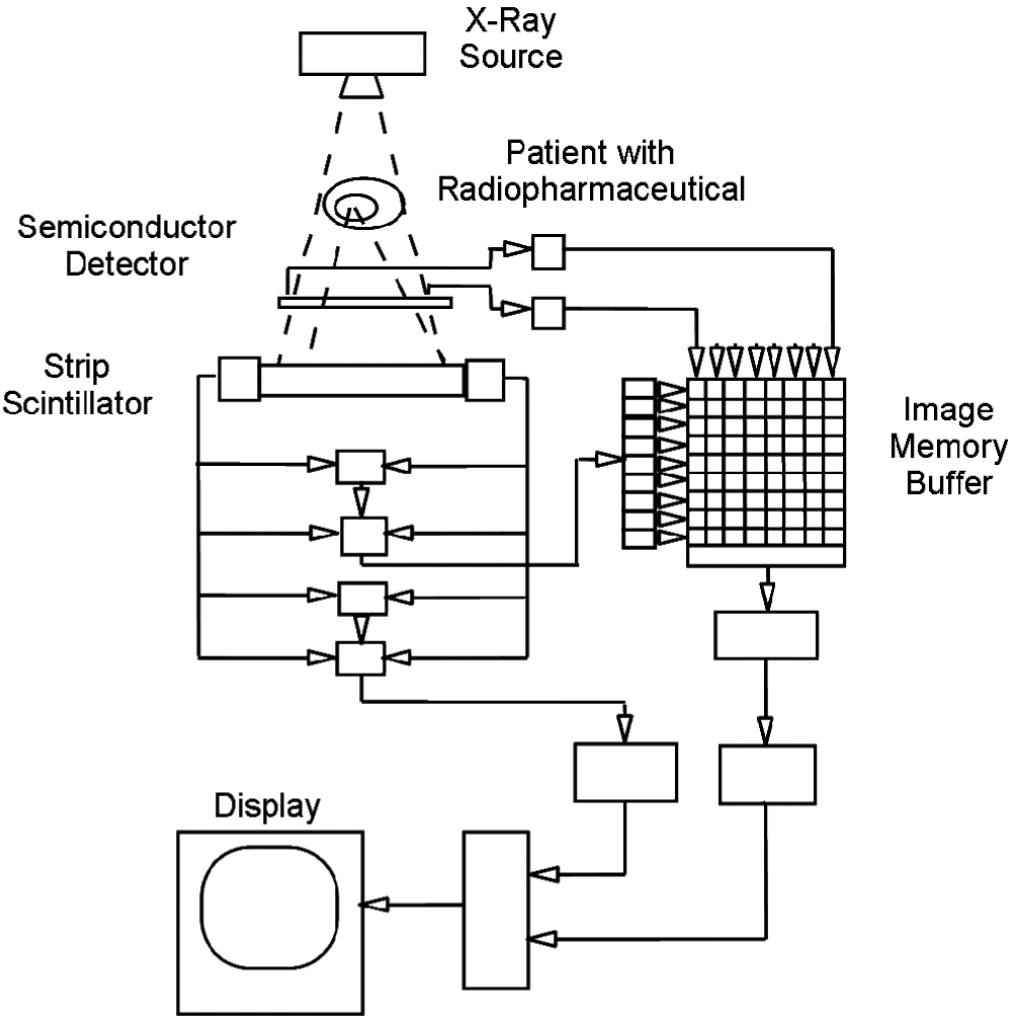

Figure 1.
Schematic of transmission-emission computer tomography system proposed by Mirshanov for simultaneous SPECT/CT with tandem semiconductor and scintillation strip detectors. (Figure from reference [227]).

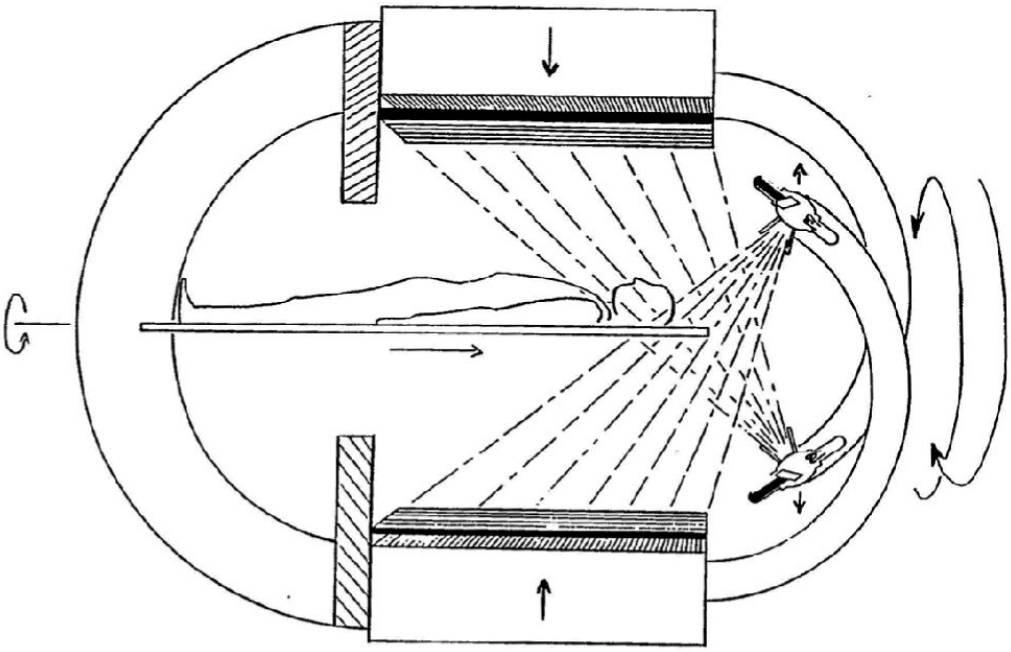

Figure 2.
Schematic of “Transmission/Emission Registered Imaging (TERI) Computed Tomography Scanner” proposed by Kaplan for simultaneous SPECT/CT imaging. (Figure from reference [44]).

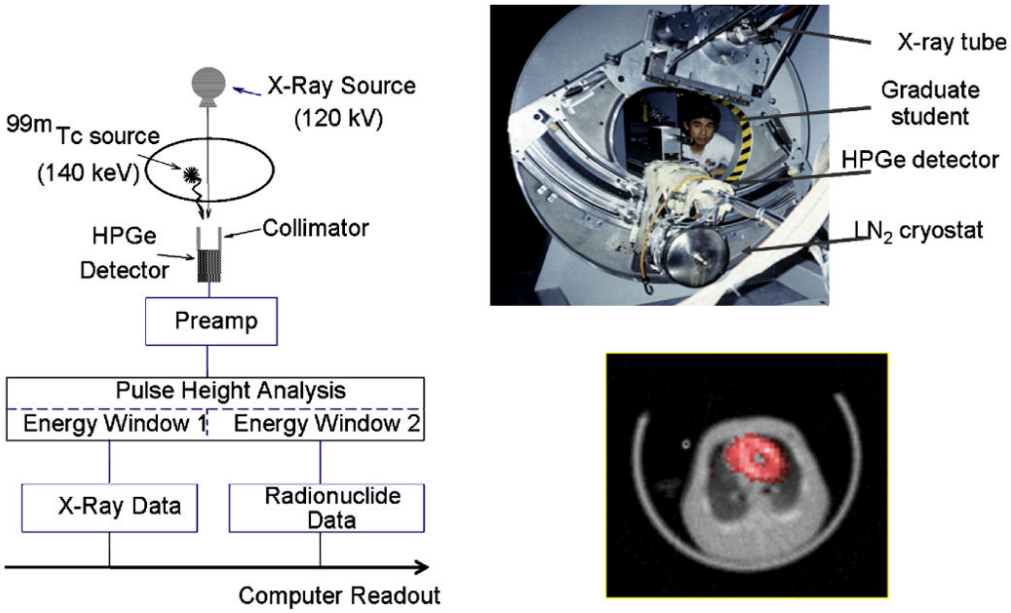

Figure 3.

(left) Schematic of data acquisition system for UCSF Emission-Transmission CT (ETCT) System. (Top right) Photograph of prototype ETCT system. (Bottom right) Transaxial image showing myocardial uptake of ^{99m}Tc-sestamibi SPECT image (red) superimposed on a gray-scale CT image of a porcine model of myocardial perfusion. (Figure on left, upper right, and bottom right reproduced with permission from references [46], [228], and [50], respectively.)

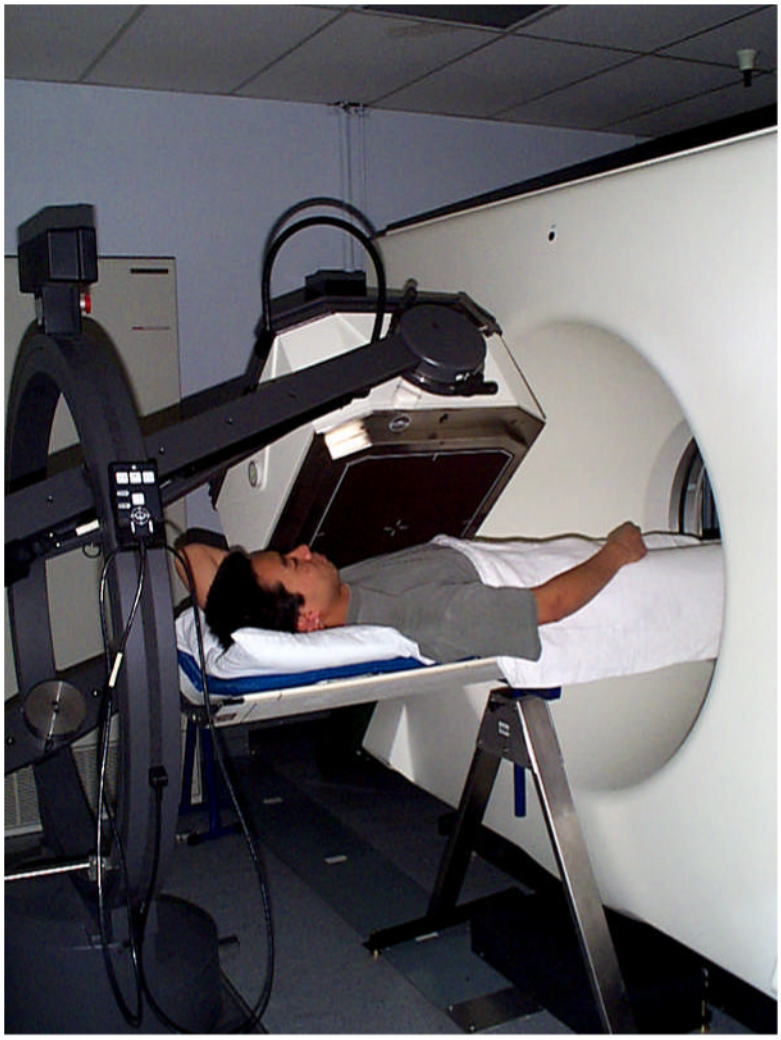

Figure 4.
Prototype SPECT/CT system configured at UCSF from GE 9800 Quick CT system and single-detector GE XR/T SPECT system. Extended table and external table support allows both SPECT and CT imaging without removing patient from system. (Reproduced with permission from reference [229]).

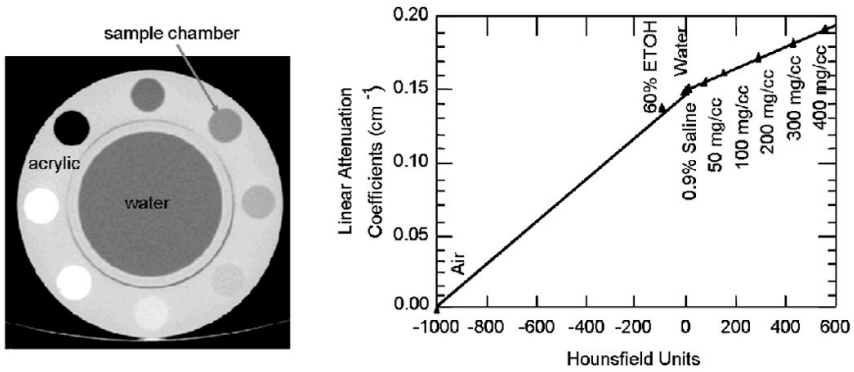

Figure 5.

Calibration of CT for x-ray derived attenuation coefficients performed with cylindrical phantom (left) containing different tissue equivalent materials. CT values (ie Hounsfield units) are correlated with values of linear attenuation coefficients (ie cm^{-1}) calculated from known composition of tissue equivalent materials calculated at energy of radionuclide used for emission imaging. Calibration curve (right) used to convert values in CT image to form patient-specific map of attenuation coefficients for attenuation correction of emission image (Reproduced with permission from reference [21]).

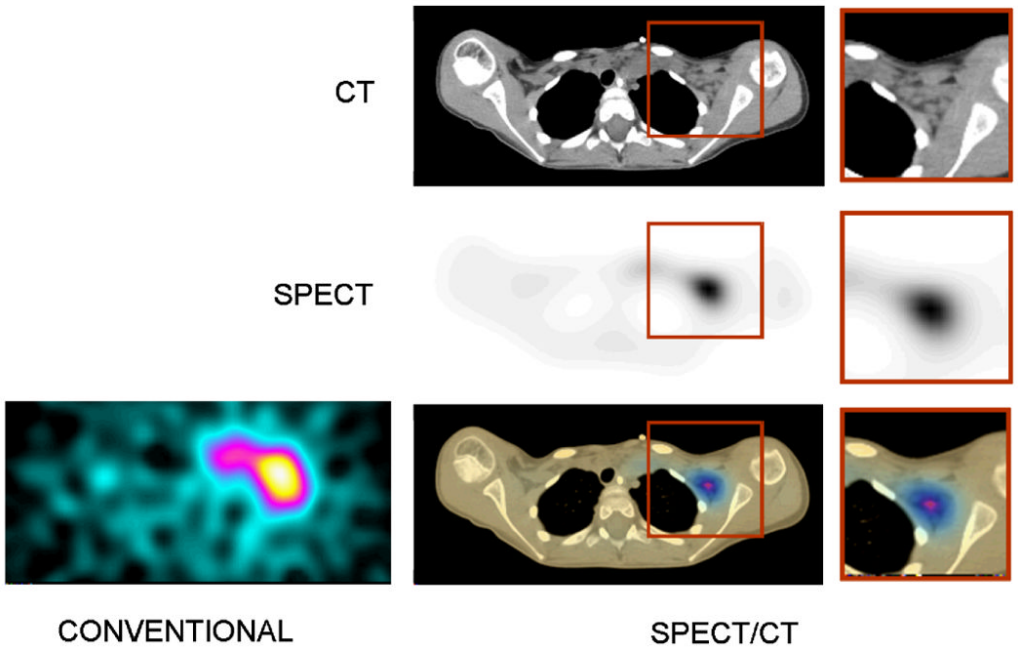

Figure 6.
Images of ^{131}I-metaiodobenzylguanidine (MIBG) of 7 year-old female with neuroblastoma with conventional SPECT (left) and CT (top right). SPECT image (middle right) and fused SPECT/CT image (bottom right) following compensation for photon attenuation and the geometrical response of the collimator (middle right). (Adapted and reproduced with permission from reference [32]).

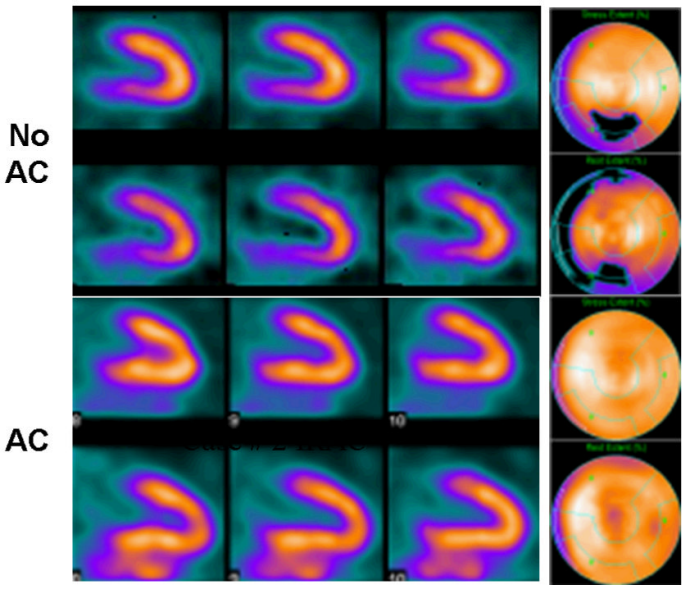

Figure 7.
^{99m}Tc-sestamibi SPECT scan of 66 year old male with atypical chest pain reconstructed using conventional filtered backprojection without attenuation correction (top) and using iterative reconstruction with x-ray based attenuation correction (bottom). Conventional perfusion SPECT showed defect in the inferior wall. Iterative reconstruction with attenuation correction produced a perfusion image which was read as being normal as was confirmed with coronary angiography. (Courtesy of General Electric Healthcare, Inc.)

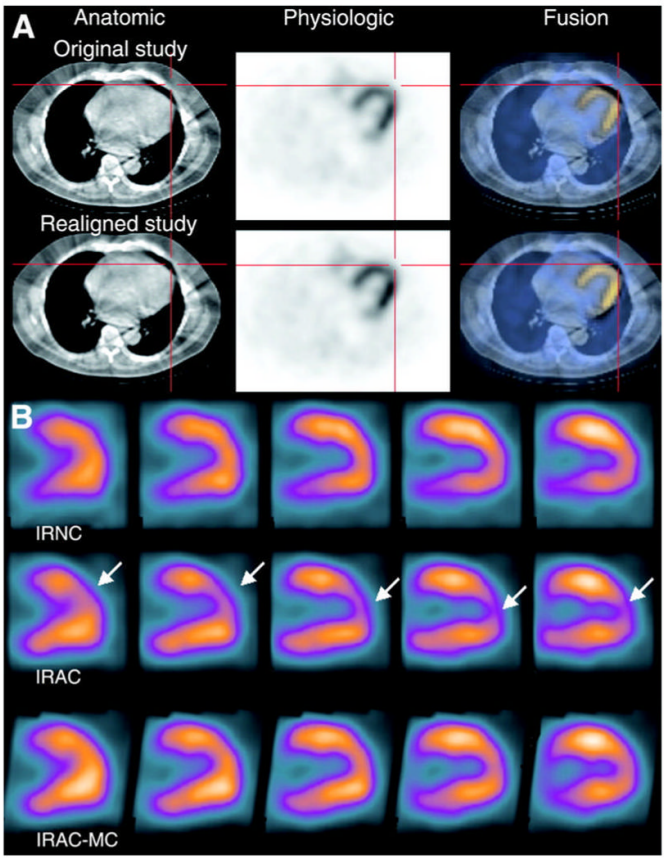

Figure 8.
(A) Co-registered CT (top), SPECT (middle), and fused SPECT/CT (bottom) myocardial perfusion images with ^{99m}Tc-sestamibi. Top row shows images with misalignment of SPECT/CT images. Bottom row show SPECT/CT images following registration using vendor-supplied software. (b) Vertical long-axis slices of ^{99m}Tc-sestamibi images without attenuation correction (IRNC), with attenuation correction of original data (IRAC), and with attenuation correction following correction for spatial misalignment (IRAC-MC). Defects in apical anterior wall of original attenuation-corrected SPECT images are not apparent in uncorrected SPECT images and in attenuation corrected SPECT images following correction for misalignment. (Reproduced with permission from reference [62]).

GE Infinia Hawkeye

Siemens Symbia

Philips Precedence

Figure 9.
Clinical SPECT/CT systems in 2007. (Top) GE Infinia Hawkeye; (Bottom left) Siemens Symbia; (Bottom right) Philips Precedence (Courtesy of GE Healthcare, Inc., Siemens Medical Solutions, Inc., Philips Medical Systems, Inc.)

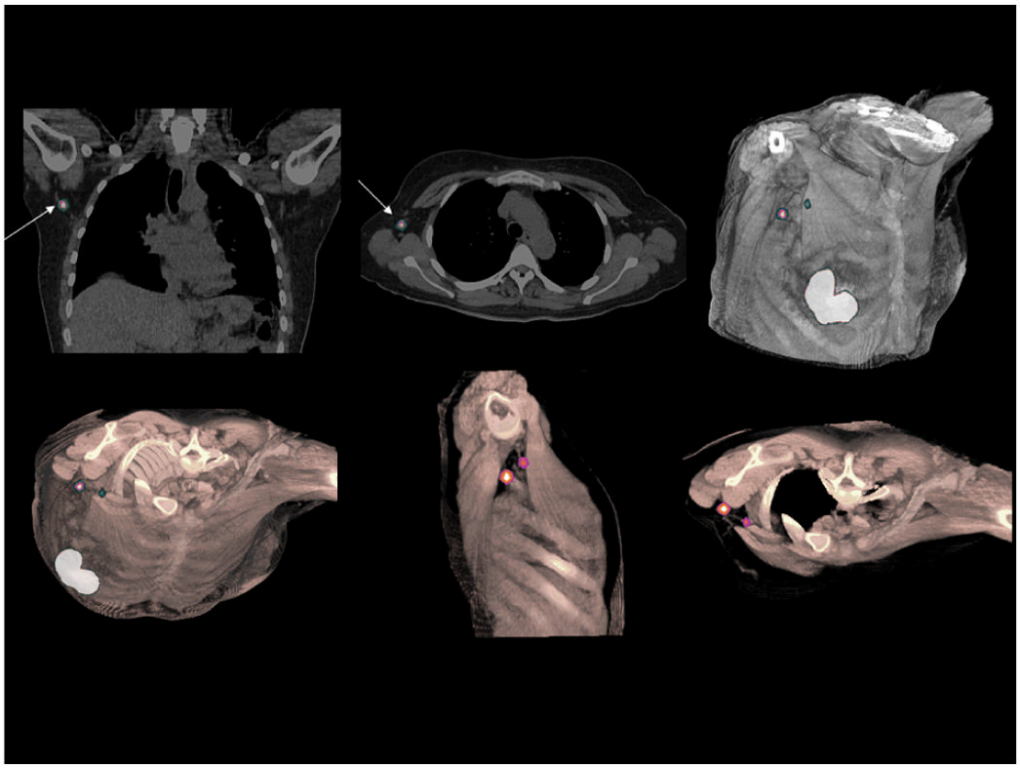

Figure 10.
Lymphoscintigraphy for sentinel node detection of patient with primary breast carcinoma. SPECT/CT study demonstrates two sentinel lymph nodes in the axilla adjacent to the trapezius and pectoralis major muscles. Volume rendering of fused datasets from thin slice spiral CT and SPECT demonstrate positions of the sentinel nodes in preparation of surgical planning for node removal. (Courtesy of Siemens Medical Solutions, Inc.)

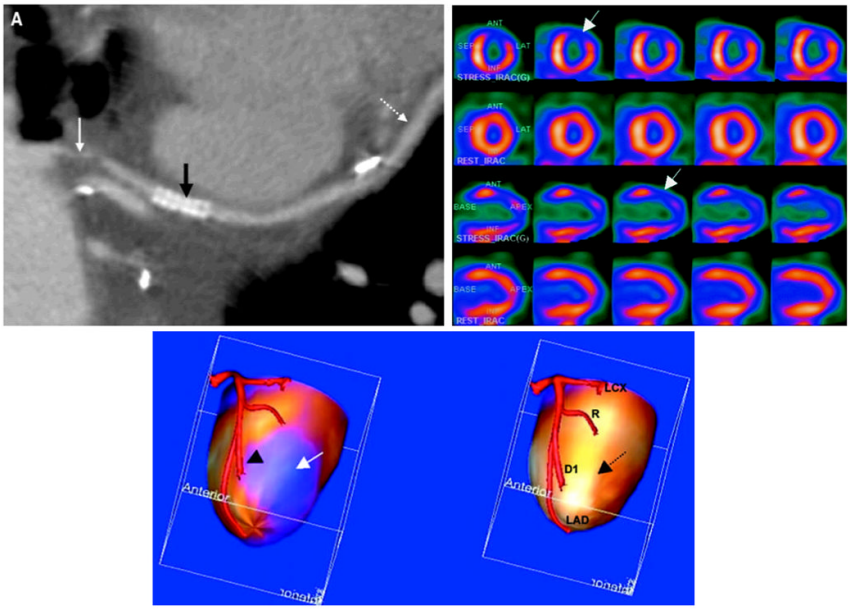

Figure 11.

CT coronary angiography (CTCA) and ^{99m}Tc-sestamibi stress/^{201}Tl rest SPECT images with x-ray based attenuation correction. Study performed with 16-slice CT scanner and dual-head variable-angle SPECT system with shared patient table to spatially register images from patient with coronary artery bypass graft. (Top left) Curved multiplanar re-formats of CTCA data shows severe irregular stenosis (solid white arrow), patient stent (black arrow), and patent diagonal artery distal to anastomosis with saphenous vein graft (dotted white arrow). (Top right) Cardiac perfusion SPECT study at stress (first and third rows) and rest (second and forth rows) shows reversible perfusion defect in the anterolateral wall (arrows) consistent with myocardial ischemia. (Bottom) Surface rendered image showing myocardial perfusion from SPECT study fused on left ventricular surface with native left coronary tree. At bottom left, decreased perfusion in the anterolateral wall (blue region, arrow) corresponds to region of first diagonal artery (arrow head). Fused data (bottom right) shows normal perfusion at rest in the same area (dotted arrow). The fused SPECT/CTCA image is consistent with myocardial ischemia related to a tight, irregular stenosis of the proximal saphenous vein graft to the first diagonal artery. LAD indicates left anterior descending coronary; D1, first diagonal branch; R, ramus intermedius coronary; and LCX, left circumflex coronary. (Adapted and reproduced permission of reference [115].)

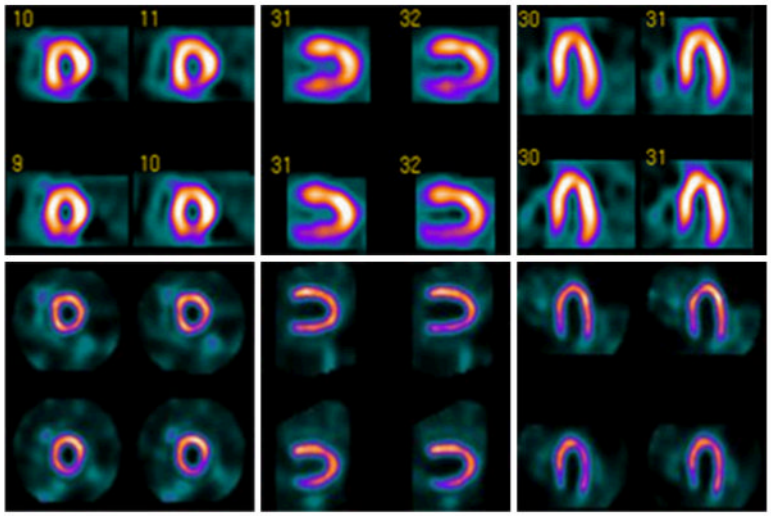

Figure 12.

^{99m}Tc-sestamibi myocardial perfusion images obtained with conventional SPECT (top) and with novel high-efficiency "D-SPECT" system (bottom) using ^{99m}Tc-sestamibi stress/rest gated protocol. High-dose (first row) and low-dose (second row) images acquired with 28 mCi and 10 mCi respectively of ^{99m}Tc-sestamibi, and required 16 min and 20 min with conventional SPECT versus 4 min and 2 min with D-SPECT. Conventional SPECT interpreted as having reversible inferior wall defect. D-SPECT interpreted as normal and was confirmed by coronary angiography. (Courtesy of Spectrum Dynamics, Ltd.)

Table 1

Clinical Applications of SPECT/CT Cited

Anatomical/Disease Site	Radiopharmaceutical	SPECT/CT Application
Adrenal masses	^{123}I-metaiodobenzylguanidine, ^{75}Se-cholesterol	Anatomical localization [161]
Biliary leak	^{99m}Tc-diisopropyl iminodiacetic acid	Anatomical localization [141]
Bone scintigraphy	^{99m}Tc-methylene diphosphonate, ^{99m}Tc-dicarboxypropane diphosphonate	Anatomical localization, attenuation correction [162-169]
Brain cancer	^{99m}Tc-tetrofosmin	Anatomical localization [170]
Breast cancer	^{99m}Tc-sestamibi	Anatomical localization [171]
Colorectal cancer	^{99m}Tc-labelled macroaggregated albumin	Hepatic artery infusion of chemotherapy [172]
Coronary artery calcification	^{99m}Tc-tetrofosmin	Coronary artery calcification correlated with myocardial perfusion imaging [120,142]
Coronary artery disease	Thallium-201, ^{99m}Tc-sestamibi, ^{99m}Tc-tetrofosmin	CT coronary artery calcification correlated with myocardial perfusion imaging [116,117,126]
Coronary artery disease, myocardial perfusion imaging	Thallium-201, ^{99m}Tc-sestamibi, ^{99m}Tc-tetrofosmin	Attenuation correction [29,60-64,114,121-124,153,173]
Coronary bypass graft	Thallium-201, ^{99m}Tc-sestamibi	Bypass grant definition and localization [115]
Crohn's disease	^{99m}Tc-HMPAO-labeled leukocytes	Anatomical localization [137]
Esophogeal cancer, adenocarcinoma of gastric cardia	^{99m}Tc-nanocolloid or ^{99m}Tc-sulfur colloid	Anatomical localization, surgical planning [174]
Head/neck cancer	L-3-^{123}I-iodine-alpha-methyl-tyrosine, ^{123}I-labeled L19(scFv)2 antibody	Anatomical localization [175-177]
Hepatic haemangioma	^{99m}Tc-labelled red blood cells	Anatomical localization [178,179]
Hepatic carcinoma	^{99m}Tc-macroaggregated albumin	Anatomical localization [180]
Human immunodeficiency virus (HIV)	^{99m}Tc-sulfur colloid	Anatomical localization of microbicide surrogate [138]
Infection	Gallium-67, ^{111}In-labeled leukocytes	Anatomical localization [133-136]
Left ventricular function	^{99m}Tc-tetrofosmin	Regional wall motion evaluation, myocardial muscle mass, ejection fraction, cardiac volumes [118]
Lung (ventilation/perfusion)	^{99m}Tc-Technegas, ^{99m}Tc-macroaggregated albumin	Anatomical localization and registration of ventilation-perfusion patterns [139,140]
Lung cancer	^{99m}Tc-sestamibi, ^{99m}Tc-depreotide	Anatomical localization [181-183]
Lymphoma	Gallium-67	Anatomical localization [184-186]
Myocardium	^{111}In-oxime-labeled mesenchymal stem cells	Stem cell imaging [187]
Neuroendocrine tumor	^{111}In-octreotide, ^{123}I-metaiodobenzylguanidine, ^{99m}Tc-depreotide	Attenuation correction, depth-dependent compensation for collimator response [32,59,75,103-105,161,188-190]
Non-Hodgkin's lymphoma	^{131}I-anti-CD20 rituximab	Radioimmunotherapy dosimetry [112]
Osteomyelitis	^{99m}Tc-labelled antigranulocyte antibodies, ^{99m}Tc-dicarboxypropane diphosphonate, ^{99m}Tc-hexamethylpropylene amine oxime (HMPAO)	Anatomical localization [129-131]

Anatomical/Disease Site	Radiopharmaceutical	SPECT/CT Application
Pancreatic carcinoma	^{99m}Tc-macroaggregated albumin	Anatomic localization, evaluation of therapeutic efficacy for pancreatic chemotherapy [180,191-193]
Parathyroid gland	^{99m}Tc-sestamibi	Anatomical localization [161,194-198]
Pheochromocytoma	^{123}I-metaiodobenzylguanidine	Anatomical localization [189]
Prostate cancer	^{111}In-capromab pendetide	Attenuation correction, anatomical localization, monitoring brachytherapy [12,26,199-204]
Sentinel lymph node biopsy (bladder cancer, head/neck carcinoma, lung cancer, melanoma, oral cavity prostate cancer, squamous cell carcinoma)	Thallium-201, ^{99m}Tc-albumin colloid (albures), ^{99m}Tc-sulfur colloid, ^{99m}Tc-tin colloid, ^{99m}Tc-colloidal human serum albumin, ^{99m}Tc-antimony sulphide colloid	Anatomical localization, attenuation correction, surgical planning [183,205-217]
Sentinel lymph node biopsy (breast cancer)	^{99m}Tc-rhenium colloid	Attenuation correction, anatomical localization [218,219]
Splenosis	^{99m}Tc-labelled colloids, ^{99m}Tc-labelled heat-damaged red blood cells	Anatomical localization [220,221]
Sympathetic nervous system tumors	^{123}I-labeled metaiodobenzylguanidine	Anatomical localization, attenuation correction [222]
Temporomandibular joint (TMJ)	^{99m}Tc-methylene diphosphonate	Anatomical localization, TMJ dysfunction [132]
Thyroid carcinoma	Iodine-131	Anatomical localization, therapeutic monitoring [161,223-225]
Whole body (phantom study)	Technetium-99m	Attenuation correction, radioimmunotherapy dosimetry [226]